AGU PUBLICATIONS

JGR

Journal of Geophysical Research: Solid Earth

RESEARCH ARTICLE

10.1002/2014JB011661

Key Points:
- First self-consistent GPS-based earthquake catalog for Sumatran plate boundary
- Thirty Sumatran earthquakes are documented
- Rich resource of spatial and temporal Sumatran earthquake cycle information

Supporting Information:
- Tables S1–S14

Correspondence to:
L. Feng,
lfeng@ntu.edu.sg

Citation:
Feng, L., E. M. Hill, P. Banerjee, I. Hermawan, L. L. H. Tsang, D. H. Natawidjaja, B. W. Suwargadi, and K. Sieh (2015), A unified GPS-based earthquake catalog for the Sumatran plate boundary between 2002 and 2013, *J. Geophys. Res. Solid Earth*, *120*, doi:10.1002/2014JB011661.

Received 16 OCT 2014
Accepted 20 APR 2015
Accepted article online 24 APR 2015

A unified GPS-based earthquake catalog for the Sumatran plate boundary between 2002 and 2013

Lujia Feng[1], Emma M. Hill[1], Paramesh Banerjee[1], Iwan Hermawan[1], Louisa L. H. Tsang[1], Danny H. Natawidjaja[2], Bambang W. Suwargadi[2], and Kerry Sieh[1]

[1]Earth Observatory of Singapore, Nanyang Technological University, Singapore, [2]Research Center for Geotechnology, Indonesian Institute of Sciences, Bandung, Indonesia

Abstract We have compiled the first self-consistent GPS-based earthquake catalog for the Sumatran plate boundary. Using continuous daily position time series from the Sumatran GPS Array (SuGAr), we document 30 earthquakes which occurred within or outside the SuGAr network from August 2002 through the end of 2013, and we provide estimates of both vertical and horizontal coseismic offsets associated with 1 *M*9.2, 3 *M*8, 6 *M*7, 19 *M*6, and 1 *M*5.9 earthquakes, as well as postseismic decay amplitudes and times associated with 9 $M > 7$ earthquakes and 1 *M*6.7 earthquake. For most of the previously studied earthquakes, our geodetic catalog provides more complete coseismic displacements than those published, showing consistent patterns of motion across a large range of distances. For many of the moderate to large earthquakes, we publish their coseismic displacements for the first time, providing new constraints on their locations and slip distributions. For the postseismic time series, we have tackled the challenge of separating the signals for individual events from the overlapping effects of many other earthquakes. As a result, we have obtained either new or much longer time series than previously published. Based on our long time series, we find logarithmic decay times ranging from several days to more than 20 years, and sometimes a second decay time is needed, suggesting that when studying large to great Sumatran earthquakes, we need to consider multiple postseismic mechanisms. Our geodetic catalog provides rich spatial and temporal Sumatran earthquake cycle information for future studies of the physics and dynamics of the Sumatran plate boundary.

1. Introduction

The Sumatran plate boundary offshore Sumatra, Indonesia, is a result of the oblique subduction of the Indian and Australian subplates beneath the Sunda plate at variable rates of 5–6 cm/yr [*DeMets et al.*, 2010]. The oblique subduction is manifested principally by two large-scale subparallel tectonic structures—the Sunda megathrust and the Sumatran fault. The Sunda megathrust primarily accommodates the trench-normal component of oblique convergence by thrust motion, while the Sumatran fault accommodates a significant amount of the trench-parallel component by right-lateral shear motion [e.g., *Fitch*, 1972; *McCaffrey*, 1991, 1992].

Despite the existence of these large-scale tectonic structures, the Sumatran plate boundary was seismically relatively inactive from 1963 to 2003 (Figure 1). According to the Advanced National Seismic System (ANSS) composite catalog (http://quake.geo.berkeley.edu/cnss/), during this 40 year period, the Sumatran plate boundary (area defined in Figure 1) experienced no *M*8, 11 *M*7, and 65 *M*6 earthquakes. In contrast, the Sumatran plate boundary has been extremely active in the decade following the 2004 M_w 9.2 Sumatra-Andaman earthquake. During this much shorter 10 year period, the area experienced 5 *M*8, 9 *M*7, and 89 *M*6 earthquakes. This recent high seismic activity has made the Sumatran plate boundary one of the most seismically active convergent plate boundaries worldwide in the time of modern observation networks.

In order to monitor this highly active plate boundary, the Sumatran GPS Array (SuGAr), a regional continuous GPS (cGPS) network, was established and continuously expanded since 2002 (Figure 2). The vast majority of the SuGAr stations are located on the Sumatran fore-arc islands and the west coast of Sumatra, directly above the Sunda megathrust and adjacent to the Sumatran fault. The SuGAr network has been able to record the spatial pattern of coseismic deformation associated with not only large to great earthquakes ($M \geq 7$) but

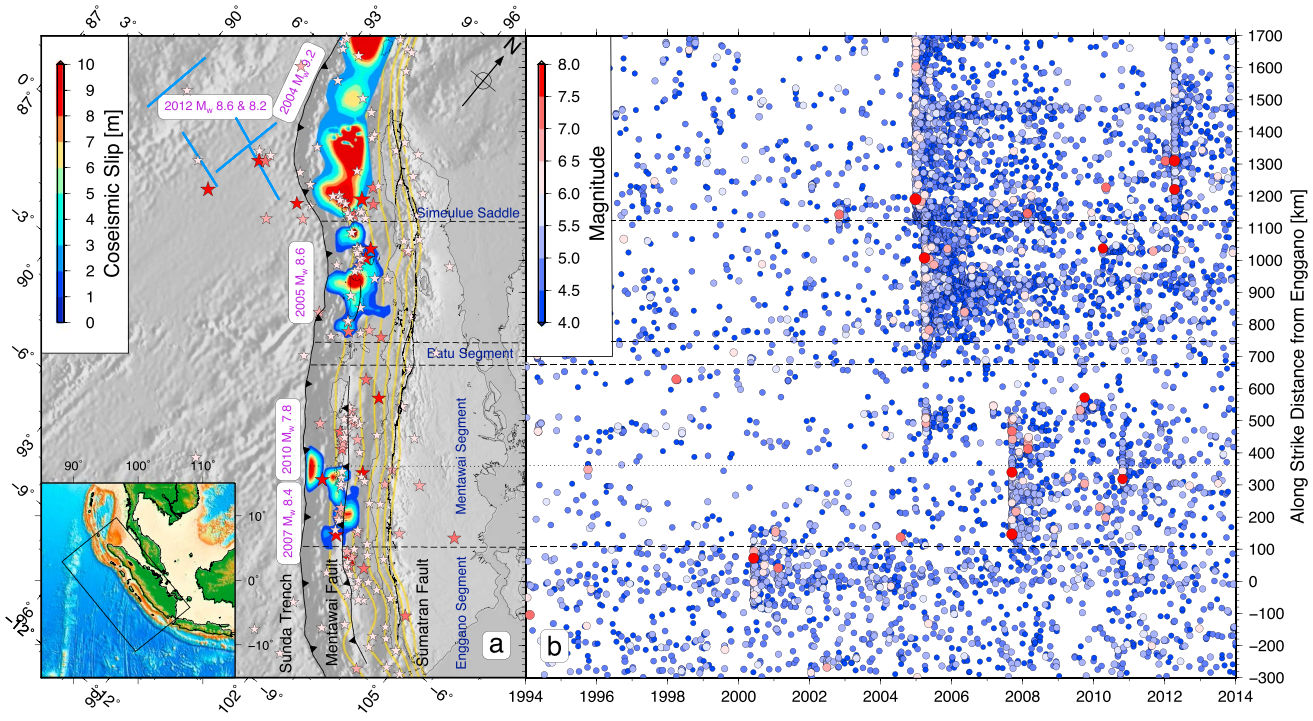

Figure 1. Earthquakes in the broad Sumatran plate boundary region, which is outlined by the black box in the inset and defined by four polygon points: [99.61°E, −11.03°S], [108.02°E, −4.22°S], [96.61°E, 9.71°N], and [88.20°E, 2.91°N]. (a) Stars represent $M \geq 6$ earthquakes from 1963 to 2013 in the Advanced National Seismic System (ANSS) composite catalog. Closed contours from north to south indicate areas of coseismic slip ≥1 m for the 2004 Sumatra-Andaman earthquake [*Chlieh et al.*, 2007], the 2005 Nias-Simeulue earthquake [*Konca et al.*, 2007], the 2010 Mentawai earthquake [*Hill et al.*, 2012], and the 2007 Bengkulu earthquake [*Konca et al.*, 2008]. Blue lines show rupture segments of the 2012 Wharton Basin earthquakes [*Hill et al.*, 2015]. Dashed black lines mark major segment boundaries along the Sunda megathrust. The dotted line separates the unbroken part of the Mentawai segment from the part that broke in the 2007 earthquake. Thin gold lines are slab contours at 20 km intervals from Slab1.0 [*Hayes et al.*, 2012]. (b) Earthquake along-strike distribution with time. Circles represent $M \geq 4$ earthquakes from the beginning of 1994 to the end of 2013. Earthquakes before 1994 are not plotted, because the spatial pattern of seismicity from 1963 to 1993 is similar to that from 1994 to 2000. Along-strike distance is referenced to a zero origin near Enggano [101.4°E, 6.1°S].

also many moderate earthquakes ($6 \leq M < 7$) in unprecedented detail. Moreover, as the SuGAr records continuously, it has also been able to record decaying postseismic deformation that occurred immediately after many Sumatran earthquakes.

To date, the SuGAr network has recorded more than a decade of daily position measurements. However, this long rich data set has not been fully analyzed yet. Previously, researchers commonly used only pieces of the SuGAr time series to study deformation associated with one or several earthquakes of their interest [e.g., *Banerjee et al.*, 2005, 2007; *Briggs et al.*, 2006; *Hsu et al.*, 2006; *Konca et al.*, 2008; *Lubis et al.*, 2013; *Wiseman et al.*, 2011, 2012], and most of these researchers estimated preseismic rates, coseismic offsets, or postseismic decays separately. Thus, to the best of our knowledge, no one has yet included preseismic rates and all the coseismic and postseismic deformation in one parameter space to fit the full time series of each SuGAr station in one single optimization procedure or tackled the challenging task of separating all the temporally and spatially varied signals in the data. Furthermore, most of the previous studies focused on great earthquakes; therefore many recorded moderate-to-large earthquakes and their ensuing postseismic deformation have never been studied or even discovered in the SuGAr time series before.

In this paper, we use nonlinear curve fitting to systematically analyze the SuGAr daily position time series for the period from August 2002 through the end of 2013, in order to consistently and completely quantify deformation from all the recorded earthquakes, including not only the great and large earthquakes but also many smaller events. After carefully identifying all the earthquakes recorded by the SuGAr, we simultaneously determine all the coseismic displacements and postseismic decays, along with long-term rates and seasonal signals, by finding the best fit of a functional representation of these contributions to the time series.

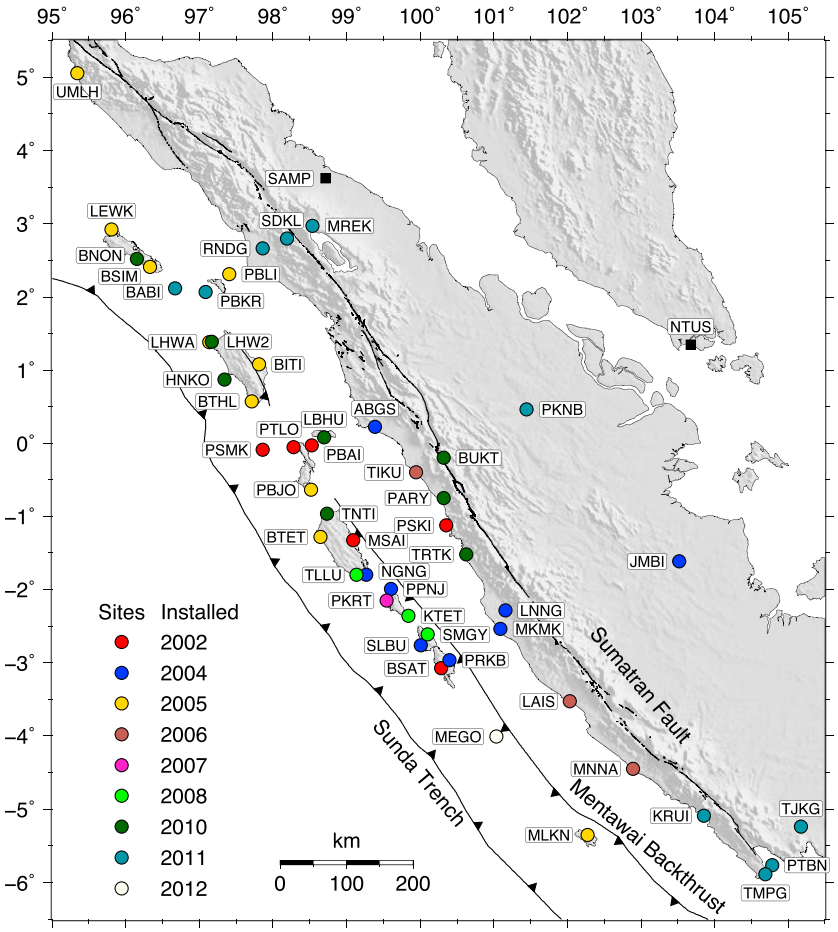

Figure 2. Map of 50 SuGAr stations. Colors indicate year of installation. Black squares represent two non-SuGAr stations installed in the late 1990s. MEGO replaced PMGT, which had only limited data from 2008 to 2009 and is not in operation any more.

Our results include (1) the first self-consistent geodetic earthquake catalog that provides a rich spatial and temporal earthquake cycle database for future studies of the physics and dynamics of the Sumatran plate boundary, (2) long-term rates that can indicate the degree of coupling on the megathrust, and (3) postfit residuals that can be used in searching for transients. In this paper, we focus only on (1), and we discuss (2) and (3) in two subsequent papers.

The main purpose of this paper is to provide a resource for researchers who wish to study and better understand Sumatran earthquakes. This resource provides researchers with coseismic offsets that can be used for modeling coseismic slip distribution. It also provides functional parameters of postseismic deformation that has had other tectonic and nontectonic signals removed as accurately and completely as possible, so this catalog is not only the geodetic equivalent of a seismic catalog but also an aseismic catalog.

2. Data and Processing

2.1. The Sumatran GPS Array

The SuGAr network was initially created through a collaboration between the Indonesian Institute of Sciences (LIPI) and the California Institute of Technology (Caltech). In 2002, the first six stations were installed at and south of the equator. More stations were installed north of the equator after the 2004 Sumatra-Andaman and 2005 Nias-Simeulue earthquakes. Continuous expansion of the network was conducted almost every year except in 2009. In 2009, LIPI's partnership with Caltech was transferred to the Earth Observatory of Singapore (EOS). From 2009 onwards, EOS and LIPI have been continuously operating and maintaining the SuGAr network. By the end of 2012, the network comprised 48 permanent GPS stations in operation, covering

the fore-arc islands from Simeulue to Enggano, the west coast of Sumatra, and parts of the Sumatran fault (Figure 2). Presently, the network consists of 60 continuous stations.

2.2. GPS Data

In this paper, we used GPS data from 37 SuGAr stations for the period from August 2002 through the end of 2013. We excluded new stations installed after 2010 but included two old stations (LHWA and PBAI) that do not exist any more. In addition, we used data from one International GNSS Service (IGS) station (NTUS) and another station (SAMP) operated by the Indonesian National Coordination Agency for Surveys and Mapping, for the period of the late 1990s to the end of 2013. The Receiver Independent Exchange Format (RINEX) files of SuGAr data are available for public download at ftp://eos.ntu.edu.sg/SugarData with a latency of 3 months. The early data are also archived at the Scripps Orbit and Permanent Array Center.

2.3. GPS Processing Strategy

We reprocessed data from a total of 39 cGPS stations (Table 1) using the GPS-Inferred Positioning System and Orbit Analysis Simulation Software (GIPSY-OASIS) version 6.2 from the Jet Propulsion Laboratory (JPL) and JPL final precise satellite orbits and clocks [*Zumberge et al.*, 1997]. IGS08 absolute phase center variations were simultaneously applied to both satellite and receiver antennas [*Schmid et al.*, 2007]. Tidal effects from solid Earth, pole, and ocean tides were modeled and corrected. Ocean tide loading was calculated by the Onsala Space Observatory (http://holt.oso.chalmers.se/loading/) using the FES2004 model with respect to the center of mass of the solid Earth, atmosphere, and ocean combined [*Lyard et al.*, 2006]. Tropospheric wet zenith delays and horizontal gradients were estimated as random-walk parameters [*Bar-Sever et al.*, 1998]. Tropospheric zenith delays were mapped to slant delays down to a minimum elevation angle of 7° using the updated Vienna mapping functions in a grid file database (VMF1GRID) [*Boehm et al.*, 2006]. Single-receiver ambiguity resolution was applied to resolve phase ambiguities [*Bertiger et al.*, 2010].

The resulting daily positions in the International Terrestrial Reference Frame 2008 (ITRF2008) [*Altamimi et al.*, 2011] were transformed to the Sunda plate reference frame [*Altamimi et al.*, 2012] for further analysis. Such reference frame transformation is always necessary to represent long-term rates and postseismic deformation, but it does not affect coseismic offset estimation in any way. The adopted ITRF2008-Sunda transformation, which was derived from only two stations and so has a relatively large uncertainty [*Altamimi et al.*, 2012], was the only one available for ITRF2008 at the time of writing.

Since we made efforts to model most nontectonic physical signals directly and in order to maximally preserve the spatial and temporal signatures of tectonic signals, we did not apply any postprocessing filtering to the daily solutions in this paper.

3. Methods

3.1. Parameterization

Our daily position time series consist of three main signals: (1) long-term rates, (2) seasonal signals, and (3) earthquake-related signals that include coseismic and postseismic deformation. For many other networks, long-term rates presumably represent background interseismic rates. However, most of the SuGAr stations were installed shortly before or even after the great earthquakes, so the rates observed here are unlikely to represent interseismic behavior. We therefore use the phrase "long term" instead of "interseismic" to describe rates in this paper.

In order to fit the time series, we used analytical expressions to parameterize each of the different signals. Long-term rates v can be simply described by a linear term vt, with t being the measurement date; annual and semiannual seasonal signals that have constant amplitudes from year to year can be expressed by sinusoidal terms $A\sin(2\pi t) + B\cos(2\pi t) + C\sin(4\pi t) + D\cos(4\pi t)$, where A, B, C, and D are amplitudes; and coseismic deformation can be represented by $OH(t - tq)$, where tq is the day of the earthquake, O is the coseismic offset, and $H(t - tq)$ is the Heaviside step function. However, postseismic deformation cannot be uniquely represented by one single form.

Postseismic deformation can be explained by different driving mechanisms. The widely accepted mechanisms include rate-and-state frictional afterslip at, updip, or downdip of coseismic rupture patches [e.g., *Marone et al.*, 1991; *Bürgmann et al.*, 2002; *Hearn et al.*, 2002; *Perfettini and Avouac*, 2004; *Barbot et al.*, 2009], poroelastic recovery due to pore fluid flow in fluid-infiltrated fault zones [e.g., *Peltzer et al.*, 1996, 1998; *Jónsson et al.*, 2003], and distributed or localized viscoelastic relaxation in the lower crust and upper mantle driven by coseismic

Table 1. Summary of GPS Stations Analyzed in This Study

		Lon	Lat	Height	ΔT[a]	Earthquakes Recorded[b]				RMS Misfit (mm)[c]			
No.	Site	(deg)	(deg)	(m)	(years)	Co	Po1	Po2	Total	Log1	Log2	Exp1–2	LogExp
1	ABGS	99.3875	0.2208	236.25	9.32	3	3	0	6	3.95	–	3.96	–
2	BITI	97.8114	1.0786	−7.07	8.08	4	2	0	6	5.40	–	5.43	–
3	BNON	96.1508	2.5208	8.25	3.08	2	1	0	3	4.11	–	4.19	–
4	BSAT	100.2846	−3.0767	6.25	11.25	6	0	2	8	5.34	5.23	5.26	5.25
5	BSIM	96.3262	2.4092	−21.26	8.90	4	3	1	8	5.10	4.98	5.01	4.97
6	BTET	98.6439	−1.2815	21.58	8.11	1	2	0	3	4.24	–	4.25	–
7	BTHL	97.7106	0.5692	67.85	8.37	3	2	0	5	4.37	–	4.38	–
8	BUKT	100.3181	−0.2019	850.22	3.86	1	1	0	2	4.50	–	4.47	–
9	HNKO	97.3407	0.8678	106.38	3.05	0	1	0	1	6.48	–	6.48	–
10	JMBI	103.5203	−1.6156	62.83	8.70	3	0	1	4	4.36	4.32	4.32	4.32
11	KTET	99.8407	−2.3625	35.20	5.90	3	2	0	5	5.27	–	5.29	–
12	LAIS	102.0339	−3.5292	20.48	7.82	3	0	1	4	4.67	4.47	4.53	4.50
13	LEWK	95.8041	2.9236	7.06	8.88	4	5	0	9	4.72	–	4.78	–
14	LHWA	97.1345	1.3835	21.73	2.55	2	1	0	3	5.57	–	6.24	–
15	LHW2	97.1703	1.3877	11.64	2.22	1	1	0	2	3.99	–	4.00	–
16	LNNG	101.1565	−2.2853	40.10	9.36	5	1	1	7	4.70	4.67	4.67	4.67
17	MKMK	101.0914	−2.5427	0.54	9.35	6	1	1	8	4.52	4.41	4.39	4.41
18	MLKN	102.2765	−5.3526	17.12	8.41	1	1	0	2	5.50	–	5.50	–
19	MNNA	102.8903	−4.4503	28.54	7.84	2	1	0	3	4.62	–	4.62	–
20	MSAI	99.0895	−1.3264	29.18	11.39	6	2	0	8	4.71	–	4.68	–
21	NGNG	99.2683	−1.7997	46.28	9.32	6	2	0	8	5.92	–	5.93	–
22	NTUS	103.6800	1.3458	75.39	12.53	2	1	1	4	4.31	4.28	4.28	4.28
23	PARY	100.3186	−0.7526	109.90	3.95	2	0	0	2	4.34	–	4.34	–
24	PBAI	98.5262	−0.0316	−1.06	3.61	2	0	1	3	4.79	4.77	4.77	4.77
25	PBJO	98.5157	−0.6365	35.91	8.38	3	1	0	4	5.24	–	5.40	–
26	PBLI	97.4053	2.3085	−9.61	8.36	1	2	1	4	4.36	4.33	4.36	4.32
27	PKRT	99.5428	−2.1514	31.82	6.30	4	2	0	6	4.65	–	4.65	–
28	PPNJ	99.6037	−1.9940	34.88	8.70	3	3	0	6	4.81	–	4.97	–
29	PRKB	100.3996	−2.9666	21.84	9.39	6	1	1	8	6.58	6.37	6.56	6.39
30	PSKI	100.3534	−1.1247	48.30	11.40	6	3	0	9	4.45	–	4.47	–
31	PSMK	97.8609	−0.0893	9.48	11.36	4	1	1	6	4.78	4.66	4.75	4.66
32	PTLO	98.2800	−0.0546	15.90	11.37	3	1	1	5	4.49	4.39	4.40	4.39
33	SAMP	98.7147	3.6216	1.89	13.21	0	2	1	3	5.11	4.94	4.96	4.95
34	SLBU	100.0097	−2.7664	2.79	9.38	4	1	2	7	4.89	4.82	4.90	4.82
35	SMGY	100.1026	−2.6145	6.94	5.93	2	1	1	4	4.86	4.80	4.85	4.80
36	TIKU	99.9442	−0.3991	18.79	4.82	3	1	0	4	4.57	–	4.72	–
37	TLLU	99.1341	−1.8003	97.91	4.99	4	0	0	4	4.43	–	4.43	–
38	TRTK	100.6242	−1.5208	125.39	3.87	1	1	0	2	4.25	–	4.27	–
39	UMLH	95.3390	5.0531	−13.87	8.89	2	1	1	4	8.09	5.81	6.03	6.13

[a] ΔT, observation time span in years.
[b] Numbers of earthquakes recorded with offsets only (Co), offsets and one postseismic decay (Po1), and offsets and two postseismic decays (Po2).
[c] Root-mean-square (RMS) misfits when using one logarithmic decay (Log1), using two logarithmic decays (Log2), using either one or two exponential decays (Exp1–2), and using one logarithmic plus one exponential decay (LogExp).

stress changes [e.g., *Nur and Mavko*, 1974; *Pollitz et al.*, 2000, 2001; *Freed and Bürgmann*, 2004]. Unequivocally discriminating between different mechanisms used to be difficult when only limited geodetic data were available [*Thatcher*, 1983; *Savage*, 1990]; however, it has become increasingly possible with an improved coverage of high-precision three-dimensional displacement data [*Hearn*, 2003; *Jónsson*, 2008]. In some cases, one mechanism and only this mechanism is adequate to explain the observations (e.g., following the 2004 M_w 6.0 Parkfield earthquake [*Freed*, 2007]); in some other cases, none of the mechanisms alone seem to fully explain all the observations (e.g., following the 2002 M_w 7.9 Denali earthquake [*Freed et al.*, 2006] and the 1999 Chi-Chi M_w 7.6 earthquake [*Rousset et al.*, 2012]). Therefore, two or more mechanisms might be involved in postseismic processes. The involved different mechanisms might be characterized by different decay times. In addition, one mechanism may not have a constant decay time but a spectrum of decay times [*Savage and Langbein*, 2008].

Despite the differences in the proposed mechanisms, the temporal evolution of postseismic deformation can be approximately described in a simple empirical form either logarithmically [$a \log(1 + \frac{t-tq}{\tau^{\log}})$] or exponentially [$b(1 - e^{-\frac{t-tq}{\tau^{\exp}}})$] [e.g., *Feigl and Thatcher*, 2006]. Here t and tq are the measurement date and earthquake date, a and b are logarithmic and exponential decay amplitudes, and $\tau^{\log}$ and $\tau^{\exp}$ are logarithmic and exponential decay times, respectively. The logarithmic dependence may at times be considered related to frictional afterslip [*Marone et al.*, 1991] or ordinary low-temperature transient creep [*Savage et al.*, 2005, 2007], while the exponential dependence may at times be considered related to viscous flow at depth [*Thatcher*, 1983]. However, no conclusive evidence can support that either form is indicative of the physical mechanism(s) behind it. We prefer to use these simple forms to represent postseismic deformation in the time series, because our purpose is not to distinguish between different mechanisms but to quantify the spatiotemporal pattern of postseismic processes.

3.2. Step 1: Earthquake Identification

Unlike time series in many other places that are dominated by linear trends, and one or two earthquakes, the SuGAr time series are punctuated by many earthquakes that are often embedded within the postseismic decay of previous earthquake(s). And postseismic decays of several earthquakes frequently overlap each other. Thus, our first challenging step was to correctly identify all the earthquakes recorded in the SuGAr time series.

In this first step, we started from the ANSS catalog for the Sumatra region in the period from August 2002 through the end of 2013. By superimposing earthquake dates in the ANSS catalog over daily position time series, we manually correlated coseismic offsets and postseismic decays with potential causative earthquakes. None of the SuGAr stations had their antennas changed by the end of 2013; thus, no offsets were caused by equipment changes. But offsets can be induced by other nontectonic causes. In order to avoid mistakenly correlating unknown nontectonic signals with earthquakes, we carefully inspected earthquake magnitude, station-epicenter distance, and sometimes time series from nearby stations when correlating a signal with an earthquake. In order to identify subtle signals, first we removed large, easily distinguishable signals by estimating offsets, and if postseismic signals existed, we also removed logarithmic or exponential terms. The identified earthquakes were then used by the following second step to form a parameter space for each station.

3.3. Step 2: Simultaneous Nonlinear Fit

In the second step, we fitted the north, east, and vertical time series of each station in a single weighted nonlinear least squares optimization procedure to simultaneously estimate (1) long-term rates, (2) annual and semiannual seasonal signals, and (3) the identified coseismic and postseismic signals from the first step. We did not consider other signals or unknown instrumental problems. Note that we modeled the seasonal signals as having fixed amplitude and phase from year to year. According to our results, the amplitudes of seasonal signals are <1 mm for horizontal and 1–2 mm for vertical, respectively. These values are small compared to amplitudes in higher latitudes [e.g., *Blewitt and Lavallée*, 2002; *Dong et al.*, 2002]; thus, seasonal signals would not significantly influence our fits.

We linked the three directional components by the same decay time τ, while τ was estimated separately for each station to represent local effects. The full observation equation for each component of one station is

$$y(t_i) = y_0 + vt_i + A\sin(2\pi t_i) + B\cos(2\pi t_i) + C\sin(4\pi t_i) + D\cos(4\pi t_i) + \sum_{j=1}^{k} O_j H(t_i - tq_j) + \sum_{j=1}^{m} a_j \log\left(1 + \frac{t_i - tq_j}{\tau_j^{\log}}\right) H(t_i - tq_j) \quad \text{and/or} \quad \sum_{j=1}^{n} b_j \left(1 - \exp\frac{tq_j - t_i}{\tau_j^{\exp}}\right) H(t_i - tq_j) + \sum_{j=1}^{l} \Delta v_j (t_i - tq_j) H(t_i - tq_j) + e_i \quad (1)$$

where t_i for $i = 1, 2, \ldots, N$ are daily solution epochs in years, y_0 is the nominal position, e_i is the error term, k is the number of coseismic offsets, m is the number of logarithmic decays, n is the number of exponential decays, and l is the number of rate changes Δv.

We modeled earthquakes based on three scenarios. First, we modeled earthquakes without clear postseismic signals as offsets only. Second, we modeled earthquakes with clear postseismic signals as offsets plus either logarithmic or exponential decays. Third, we tested whether including postseismic signals improved the fits for earthquakes with ambiguous postseismic signals. If better fits were achieved, then we considered the earthquakes to have generated postseismic deformation; otherwise, we considered the earthquakes to have generated coseismic deformation only. In total, 37 out of the 39 stations that we used for this study recorded 72 postseismic signals associated with 10 earthquakes; the remaining two stations (PARY and TLLU) recorded no postseismic signals at all (Table 1).

We tested fitting postseismic signals in up to three procedures. First, if the residual time series for the best fit model with only one postseismic decay looked reasonably flat within the scatter, we did no further testing. Second, if one postseismic decay could not provide visually adequate fits to the time series or an extremely large decay time (>1000 years) was needed to produce adequate fits, we tested whether adding a second decay improved the fits. We found that adding a second decay reduced the root-mean-square (RMS) misfits by between 0.01 and 2.28 mm for 16 stations (Table 1). Note that adding a second decay usually produced two decay times: one that was shorter than when only a single decay time was used and another that was longer than when only a single decay time was used. Third, if neither one nor two decays provided visually adequate fits to the time series or at least one extremely large decay time was needed to produce adequate fits, we tested whether using one decay plus a rate change improved the fits. The second decay might suggest at least two characteristic decay times [*Savage and Langbein*, 2008], while the rate change might indicate a slowly decaying relaxation term [*Perfettini et al.*, 2005; *Savage and Svarc*, 2009] or changes in plate coupling [e.g., *Nishimura et al.*, 2004; *Prawirodirdjo et al.*, 2010].

Next, we tested whether logarithmic or exponential decays fitted the time series better. For three quarters of the 37 stations that recorded at least one postseismic signal, logarithmic decays fitted better than exponential decays, with RMS misfits reduced on average by 0.08 mm; however, for the remaining stations, exponential decays fitted only slightly better than logarithmic decays, with RMS misfits reduced on average by 0.01 mm (Table 1). Overall, logarithmic decays fitted better than exponential decays, similar to the results of *Kreemer et al.* [2006a] for the 2005 Nias-Simeulue earthquake. For the 16 stations that needed a second decay, we further tested whether using one logarithmic decay plus one exponential decay improved the fits. We found that using logarithmic and exponential decays jointly neither systematically improved nor worsened the misfits (Table 1). As a result, for each station, we chose a preferred functional representation that used one logarithmic decay for most earthquakes and two logarithmic decays for the others. Note that in the remainder of this paper, we consider the logarithmic form only.

3.4. Outlier Detection

Before fitting the time series, we carefully inspected the data quality. First, we discarded data recorded on the day of any of the earthquakes. Second, we flagged and removed daily points that had a formal error of any component three times larger than the 95th percentile average error of the respective component. We used the remaining points for the nonlinear weighted least squares fit. After the first iteration, we identified points that deviated too much from the best fit as outliers using the Chauvenet criterion [*Taylor*, 1997]. The Chauvenet criterion states that a point can be rejected if the probability that the point deviates from the

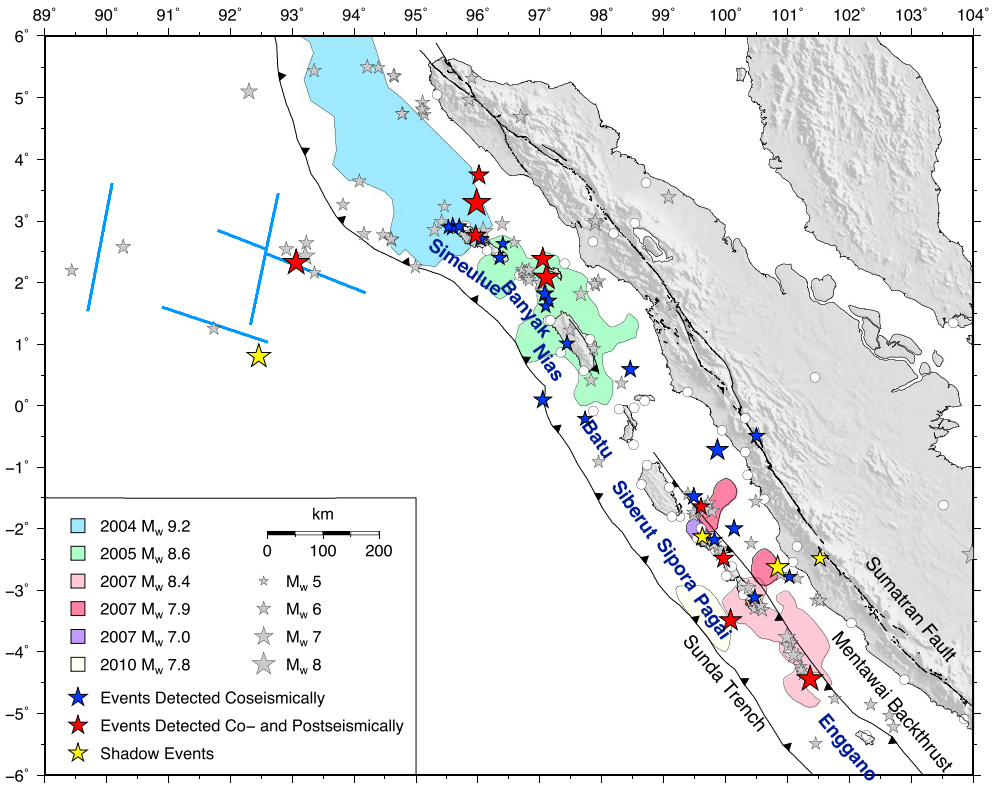

Figure 3. Thirty earthquakes were recorded by the SuGAr between 2002 and 2013. Red stars indicate 10 earthquakes for which the SuGAr detected both coseismic and postseismic deformation. Blue stars indicate 20 earthquakes for which the SuGAr detected only coseismic deformation. Yellow stars represent four shadow events whose noticeable displacements cannot be separated from a larger recorded event. Gray stars represent undetected ANSS earthquakes with magnitudes ≥5.9 between 5 August 2002 and 31 December 2013. Note that these ANSS epicenter locations are likely systematically biased [*Dewey et al.*, 2007; *Tilmann et al.*, 2010]. Colored patches delimit areas of main slip. Blue lines show rupture segments of the 2012 Wharton Basin earthquakes [*Hill et al.*, 2015]. White circles are GPS stations.

current best fit is lower than $\frac{0.5}{N}$ (N is the total number of data points). A second iteration without the outliers was conducted to achieve the final best fit results.

3.5. Error Estimation

For nonlinear curve fitting, there is no simple way to propagate uncertainties in data to uncertainties in estimated parameters, so we used the Jacobian matrix J of the final iteration to represent the error propagation from data covariance C_d to parameter covariance C_m for the preferred functional representation [*Aster et al.*, 2005].

$$C_m = J^{-g} C_d J^{-gT} \tag{2}$$

where J^{-g} is the Moore-Penrose pseudoinverse, a generalized inverse of the Jacobian matrix J.

4. Geodetic Catalog

Using the daily position time series from 39 stations, we catalog a total of 30 earthquakes with magnitudes ranging from 5.9 to 9.2, including four great earthquakes ($M \geq 8$) and six large earthquakes ($7 \leq M < 8$) (Figure 3 and Table S1 in the supporting information). Twenty out of the 30 earthquakes, including one $M > 7$ earthquake (the 2009 M_w 7.6 Padang earthquake), generated detectable coseismic offsets, but not postseismic displacements, each recorded by between 1 and 24 GPS stations. The other 10 earthquakes generated both detectable coseismic and postseismic displacements. These 10 comprised eight $M > 7$ earthquakes on the Sunda megathrust, one M_w 8.6 strike-slip earthquake under the Indian Ocean west of the Sunda trench (the 2012 Wharton Basin earthquake), and one M_w 6.7 earthquake on the Mentawai back thrust. In addition, we identify four shadow earthquakes that were large enough to generate noticeable displacements, but

whose displacements could not be separated from the signal of an earlier larger event, because the shadow events either occurred on the same day as the earlier event or fell in the early, high-rate postseismic transient of the earlier event (Figure 3 and Table S1).

Our main catalog database is presented in Tables S1–S14. In the sections immediately below, we provide summaries for each cataloged earthquake. We start from the most extensively studied great earthquakes, continue with the less extensively studied large earthquakes, and complete with the mostly never studied moderate earthquakes.

4.1. Great Earthquakes

4.1.1. The 2004 M_w 9.2 Sumatra-Andaman Earthquake

According to coseismic vertical motions derived from satellite images and microatoll measurements, the 2004 M_w 9.2 Sumatra-Andaman earthquake extended ~1600 km along the trench from under northern Simeulue at ~2.5°N to Preparis Island in Myanmar at ~14.9°N [*Meltzner et al.*, 2006]. Along this long rupture, coseismic slip was heterogeneous with distinct localized patches of high slip at different latitudes, and the largest slip exceeded more than 20 m offshore northwestern Sumatra in the south [e.g., *Subarya et al.*, 2006; *Chlieh et al.*, 2007; *Fujii and Satake*, 2007; *Rhie et al.*, 2007; *Sladen and Hébert*, 2008; *Hoechner et al.*, 2008; *Lorito et al.*, 2010]. Such long rupture and large slip generated widespread deformation on an unprecedentedly large scale, with very clear coseismic offsets (several millimeters) detected more than 3000 km away from the epicenter [*Banerjee et al.*, 2005; *Vigny et al.*, 2005; *Hashimoto et al.*, 2006; *Kreemer et al.*, 2006b].

At the time of the 2004 earthquake, only 12 SuGAr stations had been installed. Since all of them were located south of the equator, 400–800 km southeast of the southern terminus of the 2004 rupture, the recorded magnitudes of coseismic displacements were very small. Nonetheless, our estimates of coseismic horizontal offsets for these 12 stations show less spatial scatter than those of *Banerjee et al.* [2007], who estimated the offsets using data from 18 days before the earthquake to 9 days after. All of the island stations moved toward the southeast, with displacement decreasing southeastward from ~18 mm at PSMK to ~2 mm at SLBU, BSAT, and PRKB; and stations along the west coast of Sumatra moved mostly to the south, with displacement also decreasing southeastward from ~3 mm at ABGS and PSKI to ~1 mm at LNNG and MKMK (Figure 4). In general, then, all the 12 SuGAr stations moved away from the rupture, in stark contrast to most other stations in Southeast Asia (e.g., SAMP and NTUS), which moved toward the rupture area [e.g., *Banerjee et al.*, 2005; *Hashimoto et al.*, 2006; *Kreemer et al.*, 2006b]. This contrast, we suggest, may be explained by the fact that these stations are aligned with the strike of the 2004 rupture.

Besides coseismic horizontal offsets, we also provide estimates of coseismic vertical offsets at the stations, not provided by any previous studies. Our estimates show that the 12 SuGAr stations subsided by 5–10 mm, indicating a broad region of subsidence southeast of the main rupture (Figure 4).

We could not resolve any detectable postseismic transients at the 12 SuGAr stations, confirming the conclusion obtained by *Subarya et al.* [2006]; however, had postseismic motion of the millimeter scale occurred, it would have been obscured by many data gaps during that time and the large deformation caused by the 2005 Nias-Simeulue earthquake only 3 months later.

In the near field of the southern main slip patch of the 2004 rupture, three stations (UMLH, LEWK, and SAMP) among the 39 we studied revealed significant postseismic deformation. UMLH, on the west coast of northwestern Sumatra, has been continuously uplifting at ~3 cm/yr since the 2004 earthquake (Figure 5d). According to satellite imagery [*Meltzner et al.*, 2006; *Tobita et al.*, 2006] and campaign GPS measurements [*Subarya et al.*, 2006], the west coast of northwestern Sumatra subsided during the earthquake. The amount of coseismic subsidence at UMLH was likely between 23 and 58 cm, which were values recorded at the nearest campaign stations R174 and R175 [*Subarya et al.*, 2006] (Figure 5a). Therefore, the first decade of postseismic uplift at UMLH seems to have reversed all or most of the coseismic subsidence. Meanwhile, UMLH moved ~1.5 m postseismically toward the trench over the decade, which was 30–40% of the coseismic horizontal motions of R174 and R175 and nearly parallel to their coseismic directions (Figure 5a). UMLH was likely influenced by the 2005 Nias-Simeulue earthquake that occurred only 3 months later; however, we could not find any transient postseismic signal that could be associated with the 2005 earthquake, because the whole time series was dominated by the rapid and smooth 2004 postseismic decay. Separating the small contribution from the 2005 earthquake seems impossible; thus, we assume all the postseismic deformation of UMLH was caused by the 2004 earthquake.

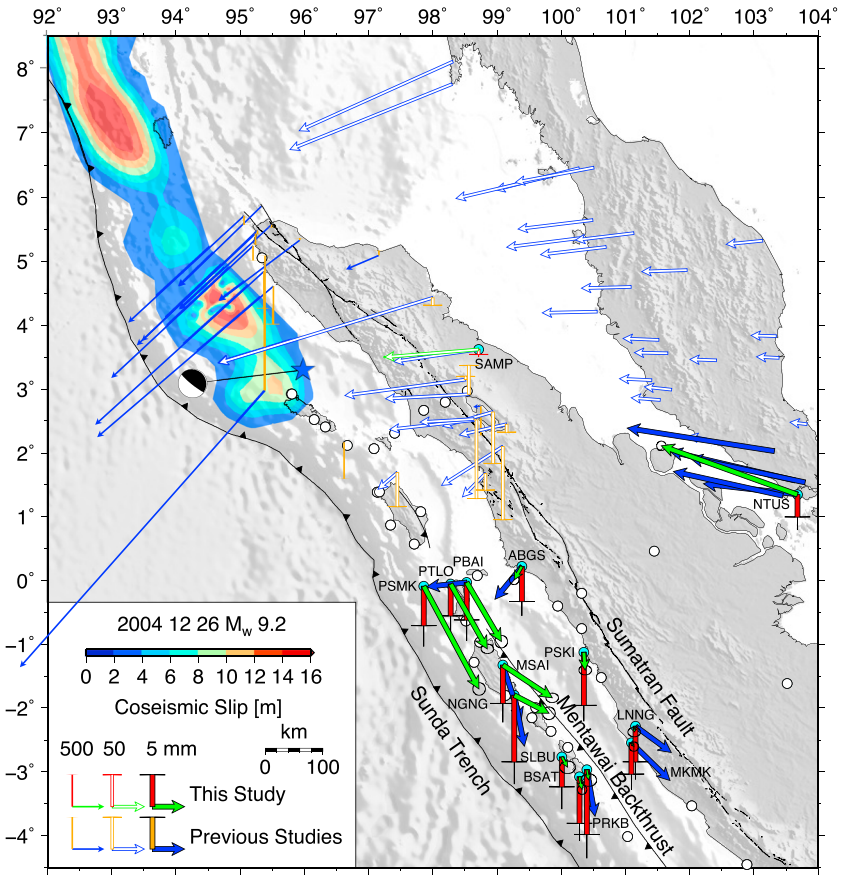

Figure 4. Coseismic deformation for the 26 December 2004 M_w 9.2 Sumatra-Andaman earthquake. Coseismic offsets are from this study or compiled by *Banerjee et al.* [2007]. Three different vector scales are used to indicate deformation across three orders of magnitude. For clarity, error ellipses are only plotted for this study, representing 95% confidence levels. Closed contours show areas of coseismic slip ≥ 1 m for the Sumatra-Andaman earthquake [*Chlieh et al.*, 2007]. Focal mechanisms taken from the global centroid moment tensor (gCMT) catalog [*Ekström et al.*, 2012] are shown at their respective gCMT locations with thin lines connecting them to their ANSS epicenter locations. Light blue and white circles are active and inactive stations during the event.

In contrast, the postseismic contributions from the 2004 and 2005 earthquakes were comparable at LEWK on the northern tip of Simeulue, which allows the separation of the two earthquakes. Due to the 2004 earthquake, LEWK moved ~0.7 m postseismically over a decade toward the trench, which amounted to only ~10% of the coseismic motion of the nearest campaign station R171 [*Subarya et al.*, 2006] (Figure 5a). The sign of postseismic vertical motion at LEWK was unclear from inspecting the raw time series visually, because the time series were affected by a M_w 6.8 event and the 2005 earthquake. However, our best fit slightly favors small postseismic subsidence at LEWK, where a coseismic uplift of 44 ± 12 cm has been suggested by a coral microatoll that was raised partially out of the water during the earthquake [*Meltzner et al.*, 2010].

UMLH and LEWK were installed almost at the same time, ~1.5 months after the 2004 earthquake, so they have no pre-earthquake measurements to directly constrain pre-earthquake long-term rates. The LEWK time series can be modeled using a combination of a postseismic transient and a linear trend that represents a long-term rate moderately modulated by postseismic displacement. In contrast, UMLH had larger postseismic displacement that obscured any linear rate. In the end, we chose not to apply any long-term rate to correct the postearthquake time series for UMLH. If any long-term rate had been removed, the amount and shape of postseismic deformation would have changed, but the change should be small compared to the large postseismic displacement at UMLH.

In our analysis, the only station that recorded both coseismic and postseismic deformation from the 2004 earthquake is SAMP, which was installed in Sampali Medan on the east coast of northern Sumatra more than 6 years before the earthquake. Over the first decade after the earthquake, the postseismic horizontal motion

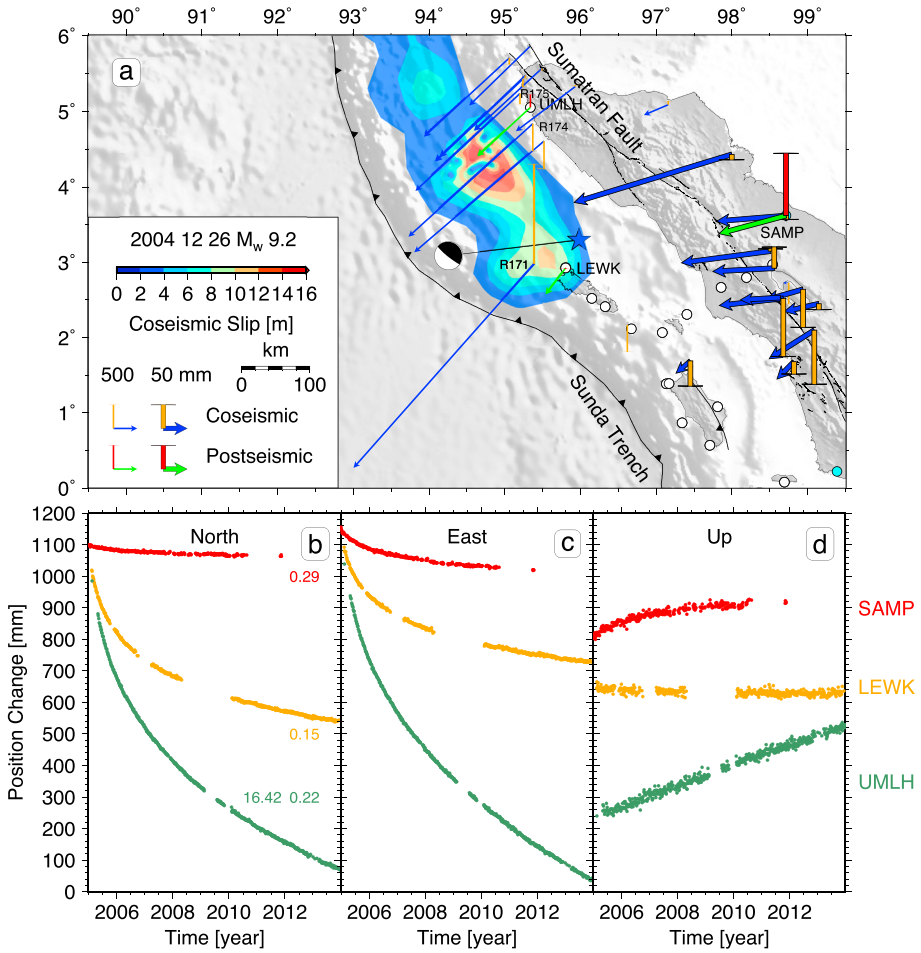

Figure 5. (a) Coseismic and postseismic deformation for the 26 December 2004 M_w 9.2 Sumatra-Andaman earthquake. Coseismic offsets are compiled by *Banerjee et al.* [2007]. Postseismic displacements up to the end of 2013 are from this study. Closed contours show areas of coseismic slip ≥1 m for the Sumatra-Andaman earthquake [*Chlieh et al.*, 2007]. (b–d) Postseismic time series for the Sumatra-Andaman earthquake. Seasonal signals, long-term rates, coseismic displacements of all the recorded earthquakes, and postseismic decays of all other earthquakes have been modeled and removed from the time series. Numbers in Figure 5b represent logarithmic time decays in years.

of ~15 cm roughly equaled the coseismic horizontal motion with trenchward direction changed only slightly, while an uplift of ~13 cm reversed and largely exceeded the small coseismic subsidence of <1 cm (Figure 5a).

Although UMLH and SAMP maintained similar coseismic and postseismic horizontal directions, their vertical motions reversed from coseismic subsidence to postseismic uplift. According to satellite imagery [*Meltzner et al.*, 2006; *Tobita et al.*, 2006] and one cGPS station ACEH, which was installed a few months after the earthquake [*Gunawan et al.*, 2014], a similar reversal from coseismic subsidence to postseismic uplift was also recorded in Banda Aceh on the northernmost tip of Sumatra. In addition, similar postseismic trenchward motion and uplift were observed in the Andaman and Nicobar Islands [*Paul et al.*, 2007, 2012; *Gahalaut et al.*, 2008]. In contrast, postseismic trenchward motion and subsidence up to 1 cm/yr were observed in Peninsular Malaysia and Thailand [*Panumastrakul et al.*, 2012; *Satirapod et al.*, 2013].

To explain not all but some of the aforementioned observations, afterslip on the megathrust [e.g., *Vigny et al.*, 2005; *Hashimoto et al.*, 2006; *Chlieh et al.*, 2007; *Paul et al.*, 2007; *Gahalaut et al.*, 2008], viscoelastic relaxation [e.g., *Pollitz et al.*, 2006, 2008; *Han et al.*, 2008; *Einarsson et al.*, 2010; *Hoechner et al.*, 2011], and poroelastic recovery [e.g., *Ogawa and Heki*, 2007; *Hughes et al.*, 2010] have been invoked individually. Using 3D finite element models, *Hughes et al.* [2010] found pore pressures recovered quickly within several months, and the magnitude of poroelastic deformation was only one fifth of viscoelastic deformation. Therefore, poroelastic effects can explain only a small fraction of early postseismic deformation and are usually disregarded in postseismic studies of the 2004 earthquake. Most recent postseismic studies of the 2004 earthquake supported the idea

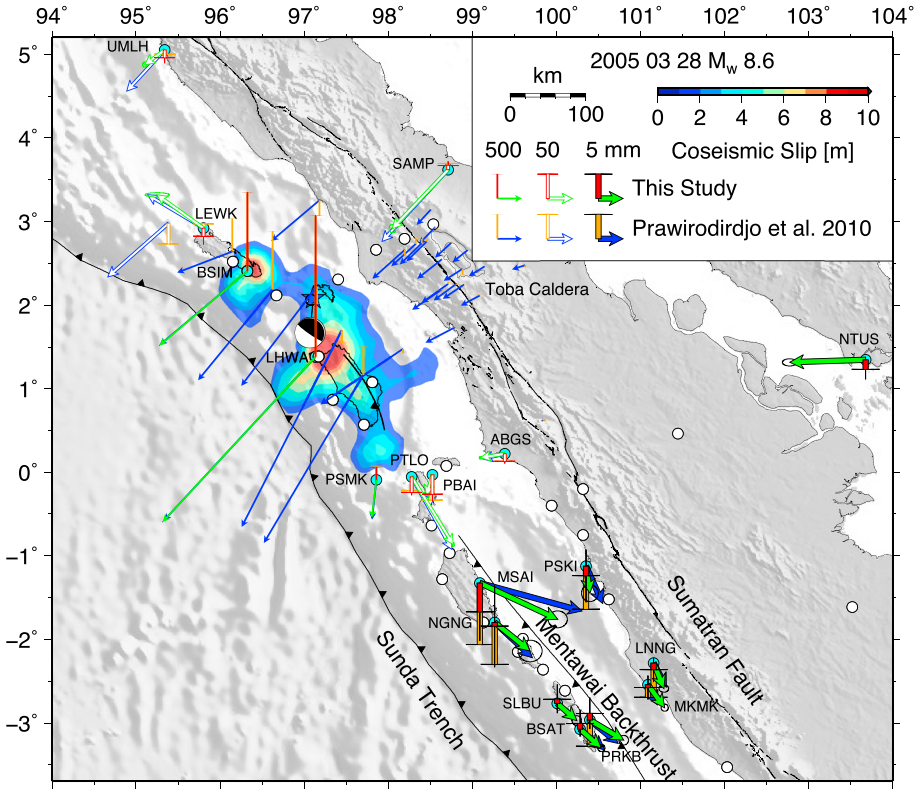

Figure 6. Coseismic deformation for the 28 March 2005 M_w 8.6 Nias-Simeulue earthquake. Closed contours show areas of coseismic slip ≥ 1 m for the Nias-Simeulue earthquake [*Konca et al.*, 2007]. See Figure 4 for similar captions.

that a combination of afterslip and viscoelastic relaxation is necessary to account for all the observations [e.g., *Panet et al.*, 2010; *Hu and Wang*, 2012; *Paul et al.*, 2012; *Satirapod et al.*, 2013; *Gunawan et al.*, 2014].

However, the relative contributions from afterslip and viscoelastic relaxation are not well constrained and remain controversial. Determining the relative contributions is particularly important for the region under northern Simeulue and the Simeulue Basin, where a significant amount of strain is potentially still stored along the megathrust after the 2004 earthquake [*Meltzner et al.*, 2010]. *Meltzner et al.* [2010] speculated that a second earthquake might occur in the coming decades to release this unreleased strain. If deep afterslip predominated the postseismic signal until now, the unreleased strain could have been partially or completely released aseismically. To fully address this question, postseismic models that combine all the available data are needed.

4.1.2. The 2005 M_w 8.6 Nias-Simeulue Earthquake

The 2005 M_w 8.6 Nias-Simeulue megathrust rupture nucleated near the Banyak Islands at about the same depth (~30 km) as the 2004 Sumatra-Andaman earthquake, propagated bilaterally, and ruptured a 400 km strip of the Sunda megathrust [e.g., *Lay et al.*, 2005; *Briggs et al.*, 2006; *Konca et al.*, 2007; *Walker et al.*, 2005; *Ishii et al.*, 2007]. The nucleation zone was a low-slip region separated along strike by two high-slip patches that have a peak slip of 8 and 11 m, respectively, beneath southern Simeulue and northern Nias [*Briggs et al.*, 2006; *Hsu et al.*, 2006]. Along dip, coseismic slip was concentrated under the fore-arc basins and islands and tapered to zero before it reached the trench [*Briggs et al.*, 2006; *Hsu et al.*, 2006; *Konca et al.*, 2007].

We detected clear coseismic offsets at all SuGAr stations operating at that time. Our estimates for the SuGAr stations are generally similar to those published by previous studies [*Kreemer et al.*, 2006a; *Konca et al.*, 2007; *Prawirodirdjo et al.*, 2010] (Figure 6).

Observed coseismic uplift, up to 2.9 m at LHWA, was concentrated in a narrow trench-parallel belt along the fore-arc islands from southern Simeulue to south of Nias. In contrast, coseismic subsidence from a few millimeters to 1 m was observed across the remainder of the fore-arc region. In the back-arc region near Toba Caldera, coseismic vertical motion was ambiguous, with some campaign stations showing uplift and others showing subsidence [*Prawirodirdjo et al.*, 2010]. The campaign measurements were likely affected by the postseismic

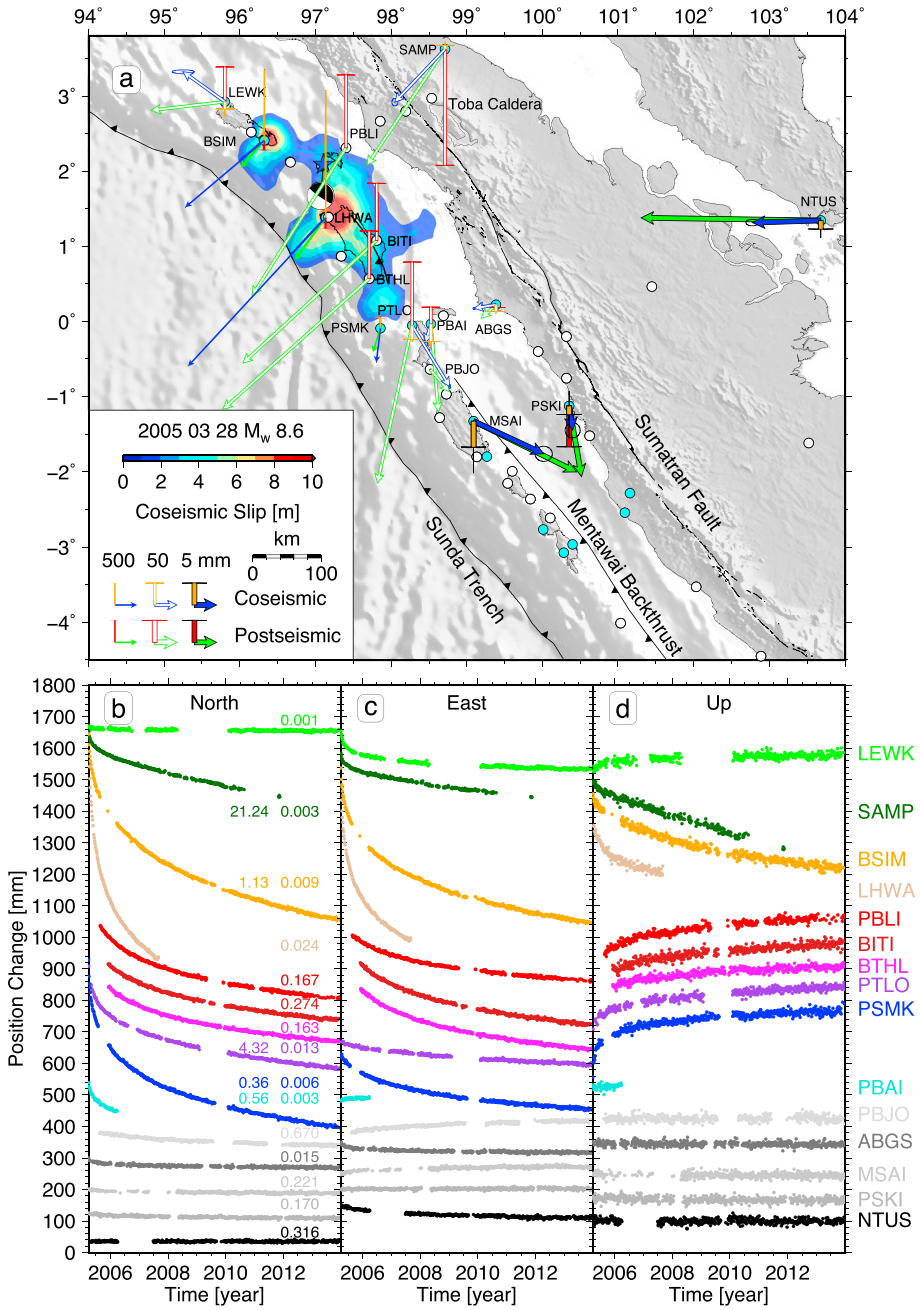

Figure 7. (a) Coseismic and postseismic deformation for the 28 March 2005 M_w 8.6 Nias-Simeulue earthquake. Coseismic offsets and postseismic displacements up to the end of 2013 are from this study. Closed contours show areas of coseismic slip ≥1 m for the Nias-Simeulue earthquake [*Konca et al.*, 2007]. (b–d) Postseismic time series for the Nias-Simeulue earthquake. See Figure 5 for similar captions.

deformation of the 2004 and 2005 earthquakes. North of Toba Caldera, the cGPS station SAMP likely uplifted coseismically by a small amount, but this coseismic uplift was soon reversed by postseismic subsidence.

We identified noticeable postseismic displacements at 15 stations (Figure 7). In general, stations in the coseismic uplift area had the largest postseismic displacements; however, their cumulative postseismic displacements were still much smaller than their coseismic displacements, even after more than 8 years by the end of 2013. On the contrary, almost all the stations in the coseismic subsidence area had accumulated much larger postseismic displacements than their coseismic displacements, both horizontally and vertically. The postseismic azimuths were either slightly or significantly different from the coseismic azimuths, and the

postseismic verticals switched to the opposite direction to the coseismic verticals at most stations except at four stations (PSMK, ABGS, MSAI, and PSKI).

The postseismic deformation for the 2005 earthquake has been modeled as afterslip [*Hsu et al.*, 2006; *Kreemer et al.*, 2006a; *Hashimoto et al.*, 2006; *Prawirodirdjo et al.*, 2010]. Using the first 11 months of GPS data, *Hsu et al.* [2006] found that extensive afterslip occurred updip, downdip, and south of the main rupture patch, in the regions where coseismic slip was small or absent. The existence and extent of the downdip afterslip were only loosely constrained by one single station (SAMP) on mainland Sumatra. When including more campaign stations on mainland Sumatra, *Prawirodirdjo et al.* [2010] estimated more deep afterslip than did *Hsu et al.* [2006]. Based on static inversion of incremental displacements in different periods, *Prawirodirdjo et al.* [2010] suggested afterslip progressed spatially over time. When switching to time-dependent inversion using the Extended Network Inversion Filter, *Hsu et al.* [2006] showed the spatial pattern of afterslip remained stationary over 11 months. Considering this stationary spatial pattern, *Kreemer et al.* [2006a] assumed one common decay time for all the time series they used and obtained 6.2 ± 0.1 days as the logarithmic decay time. Conversely, we estimated decay times separately for different stations and found all have short logarithmic decay times of several days to several months (Figure 7b). Such a short timescale likely indicates the importance of afterslip. Yet the importance of viscoelastic relaxation should not be overlooked.

Although several previous geodetic studies claimed no evidence for viscoelastic relaxation in the GPS time series of less than 1 year after the 2005 earthquake [*Hsu et al.*, 2006; *Kreemer et al.*, 2006a; *Hashimoto et al.*, 2006; *Prawirodirdjo et al.*, 2010], we found viscoelastic relaxation is important in our much longer records. The strongest evidence for viscoelastic relaxation is that SAMP required a second decay time of 21 ± 5 years to better fit its time series (Figure 7b). Additionally, PTLO needed a second decay time of ~4 years (Figure 7b). Such a long timescale is difficult to explain with afterslip only, suggesting viscoelastic relaxation as a mechanism. SAMP and PTLO were both installed several years before the 2004 and 2005 earthquakes; thus, their long-term rates can be relatively well constrained. Unfortunately, most other stations were all installed shortly after the 2004 or 2005 earthquake, so their long-term rates can be only roughly estimated using the postearthquake data. A decay with a large timescale resembles a linear trend in a short period; thus, such decay can be easily mapped into long-term rates. This could explain why only SAMP and PTLO required a second long decay time. But SAMP required a much longer decay time than PTLO. We speculate that SAMP probably recorded the viscoelastic effects from both the 2004 and 2005 earthquakes. Even though the short-time effects due to the two earthquakes can be separated using the 3 month time series in between, the long-term effects are almost impossible to be separated when the two occurred so close in space and time. Therefore, the 21 year decay time is probably a combined result of the two earthquakes. Clearly, the postseismic deformation of the 2005 earthquake needs to be reanalyzed by combining afterslip and viscoelastic relaxation.

4.1.3. The 2007 M_w 8.4 Bengkulu Earthquake

On 12–13 September 2007, several discrete patches within the Mentawai segment of the Sunda megathrust failed subsequently from southeast to northwest. First, the 2007 M_w 8.4 Bengkulu rupture nucleated halfway between Enggano and South Pagai and propagated ~200 km unilaterally to the northwest; about 12 h later, a deeper M_w 7.9 earthquake initiated next to the northeastern edge of the main rupture and jumped ~130 km farther northwest to northeast of Sipora; another 4 h later, a third M_w 7.0 earthquake occurred underneath northern Sipora [e.g., *Konca et al.*, 2008; *Borrero et al.*, 2009]. Coseismic static slip models derived from GPS, interferometric synthetic aperture radar, and coral microatoll measurements showed a patchy slip distribution, with the largest slip of ~8 m under southern South Pagai and the second largest slip of ~5 m at ~ 4°S near Mega Island, about 70 km northwest of the epicenter [*Konca et al.*, 2008].

Our coseismic offsets, representing the cumulative effects of these three 2007 earthquakes, are generally consistent with the estimates from *Konca et al.* [2008] (Figure 8). Coseismic trenchward motions were observed at most stations, with the largest reaching ~1.8 m at PRKB (not BSAT as *Konca et al.* [2008] stated). However, four island stations (MSAI, BTET, PBJO, and MLKN) far along strike from the megathrust rupture moved several millimeters to several centimeters, nearly parallel to the trench and away from the rupture source. Coseismic uplift was measured at most island stations except at the four aforementioned stations. The maximum GPS uplift was 0.75 m at BSAT from this study, while the maximum coral uplift was 1.3 m on Mega Island [*Konca et al.*, 2008]. In contrast, widespread coseismic subsidence was observed at all mainland stations, from 19 cm at MKMK to 5 mm at ABGS, except at JMBI where almost zero vertical change was recorded.

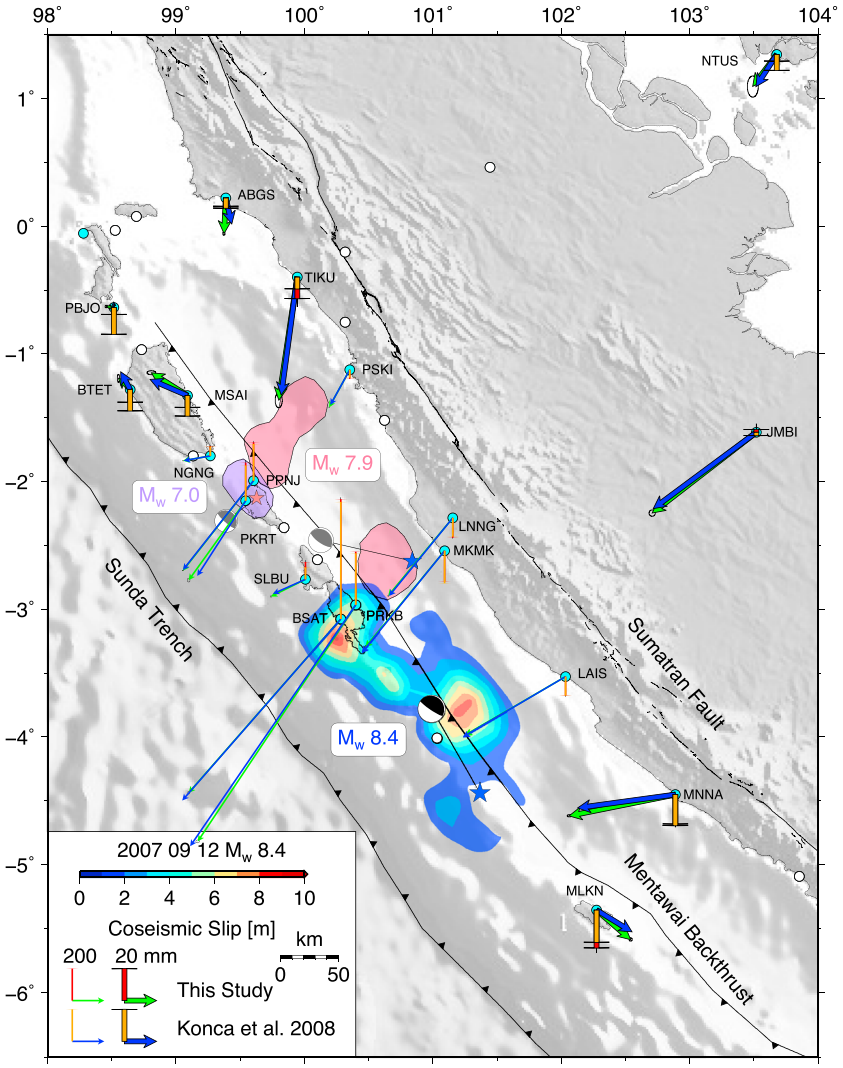

Figure 8. Combined coseismic deformation for the 12 September 2007 M_w 8.4 Bengkulu earthquake and the M_w 7.9 and M_w 7.0 aftershocks. Closed contours show areas of coseismic slip ≥1 m for the Bengkulu earthquake [*Konca et al.*, 2008]. See Figure 4 for similar captions.

We identified notable postseismic displacements at 18 stations (Figure 9). The cumulative postseismic displacements by the end of 2013 were smaller than the coseismic displacements at most stations except for five stations far from the rupture (BTET, MSAI, MLKN, JMBI, and NTUS). Postseismic horizontal motions roughly continued in the same coseismic directions except that MLKN shifted its direction of motion counterclockwise 90° toward the northwest. Postseismic uplift was found at most stations in our analysis. As opposed to our results, postseismic subsidence was previously reported for all the stations based on the first 15 months of data [*Lubis et al.*, 2013]. In comparison with the 2004 and 2005 earthquakes for which postseismic uplift was found near the main ruptures, it is difficult to explain why the 2007 earthquake caused only postseismic subsidence. Because incorrect vertical values were used when concluding that the poroelastic, afterslip, and viscoelastic effects are all necessary to be considered for the 2007 earthquake [*Lubis et al.*, 2013], this conclusion may or may not hold. In our analysis, we discovered logarithmic time decays ranging from several days up to several years, likely indicating different mechanisms (Figure 9b).

Next, we move on to discuss MLKN, which sits on the southernmost island of the Sumatran fore arc, Enggano. The motion of MLKN after the 2007 earthquake was anomalous with a clear abrupt rate change in both horizontal and vertical components before and after the 2007 earthquake. Especially, the subsidence rate changed from 5.3 ± 0.5 mm/yr to 9.4 ± 0.2 mm/yr. We could not fit such an abrupt rate change well using either one or two logarithmic decays that had reasonable decay times. An extremely large decay time of more

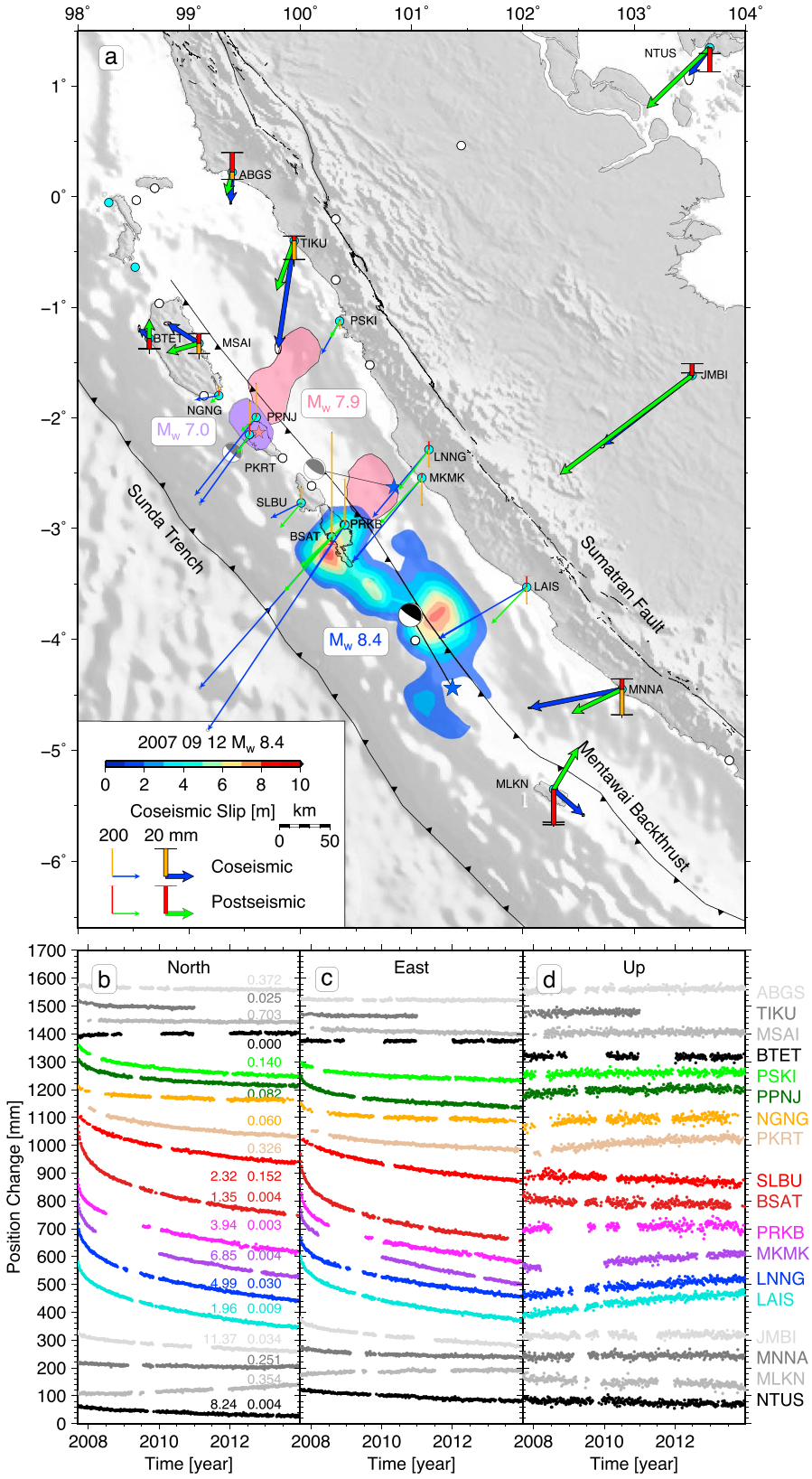

Figure 9. (a) Coseismic and postseismic deformation for the 12 September 2007 M_w 8.4 Bengkulu earthquake and the M_w 7.9 and M_w 7.0 aftershocks. Coseismic offsets and postseismic displacements up to the end of 2013 are from this study. Closed contours show areas of coseismic slip ≥1 m for the Bengkulu earthquake [*Konca et al.*, 2008]. (b–d) Postseismic time series for the Bengkulu earthquake. See Figure 5 for similar captions.

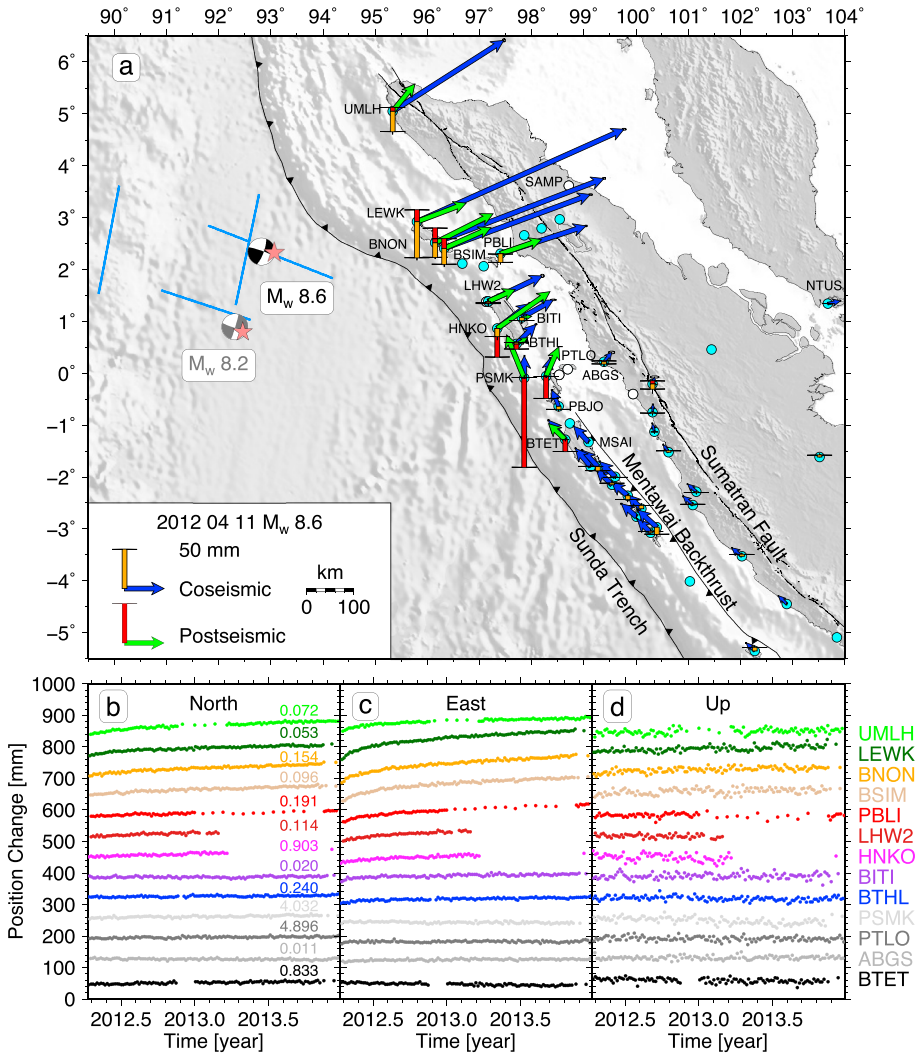

Figure 10. (a) Coseismic and postseismic deformation for the 11 April 2012 M_w 8.6 Wharton Basin earthquake and the M_w 8.2 aftershock. Coseismic offsets and postseismic displacements up to the end of 2013 are from this study. Blue lines show rupture segments of the 2012 Wharton Basin earthquakes [*Hill et al.*, 2015]. (b–d) Postseismic time series for the Wharton Basin earthquakes. See Figure 5 for similar captions.

than 5000 years was always needed if we did not include a rate change term. Because the azimuth of the horizontal rate change pointed toward the northeast and the subsidence rate increased (Figure 9a), the rate change could reflect aseismic slip on the Mentawai back thrust or enhanced coupling on the megathrust after the 2007 earthquake. Some change may also have occurred after the 2000 M_w 7.9 Enggano earthquake, because the horizontal motion of Enggano changed from more northerly in the period of 1991–2001 to almost trench-parallel in the period of 2001 to 2007 [*Prawirodirdjo et al.*, 2010]. It is possible that the 2000 earthquake caused some patch near Enggano to have a period of slipping freely, which was terminated by the 2007 earthquake.

In conclusion, the 2007 sequence caused several patches within or outside the main rupture to slip separately at different speeds and in different periods. This complex spatiotemporal slip history needs to be better understood.

4.1.4. The 2012 M_w 8.6 Wharton Basin Earthquake

The 2012 M_w 8.6 Wharton Basin earthquake occurred in the oceanic plate within a diffuse deformation zone between the Indian and Australian subplates, followed 2 h later by a M_w 8.2 aftershock that occurred ~180 km to the south. The main shock was the largest instrumentally recorded strike-slip and intraplate earthquake. This event was remarkably complex, involving many fault segments with ruptures potentially extending

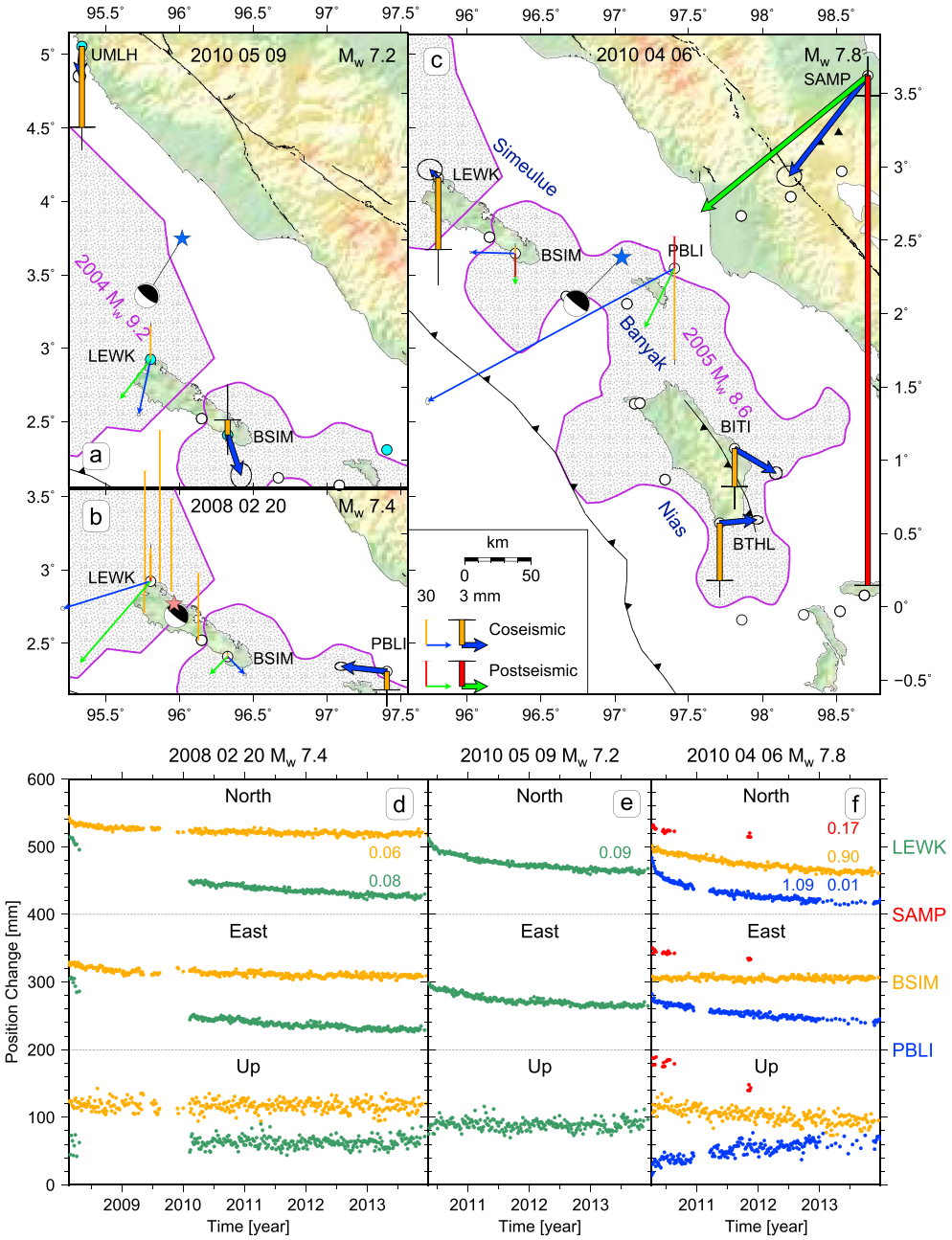

Figure 11. Coseismic and postseismic deformation for (a) the 9 May 2010 M_w 7.2 Simeulue earthquake, (b) the 20 February 2008 M_w 7.4 Simeulue earthquake, and (c) the 6 April 2010 M_w 7.8 Banyak earthquake. Coseismic offsets and postseismic displacements up to the end of 2013 are from this study. (d–f) Postseismic time series for these three large earthquakes. See Figure 5 for similar captions.

through the thin oceanic crust and penetrating significantly into the uppermost mantle [*Yue et al.*, 2012; *Meng et al.*, 2012; *Duputel et al.*, 2012; *Wei et al.*, 2013; *Hill et al.*, 2015]. Whether the majority of moment release for this event was on the old prominent NNE trending left-lateral faults or young unmapped WNW trending right-lateral faults has been debated, with some studies preferring the former [e.g., *Satriano et al.*, 2012; *Wei et al.*, 2013; *Geersen et al.*, 2015] and others preferring the latter [e.g., *Yue et al.*, 2012; *Duputel et al.*, 2012; *Hill et al.*, 2015].

Even though this earthquake occurred far west of Sumatra, with its distance to the SuGAr stations ranging from 300 to 1300 km, the whole SuGAr network recorded clear static coseismic displacements, with the largest

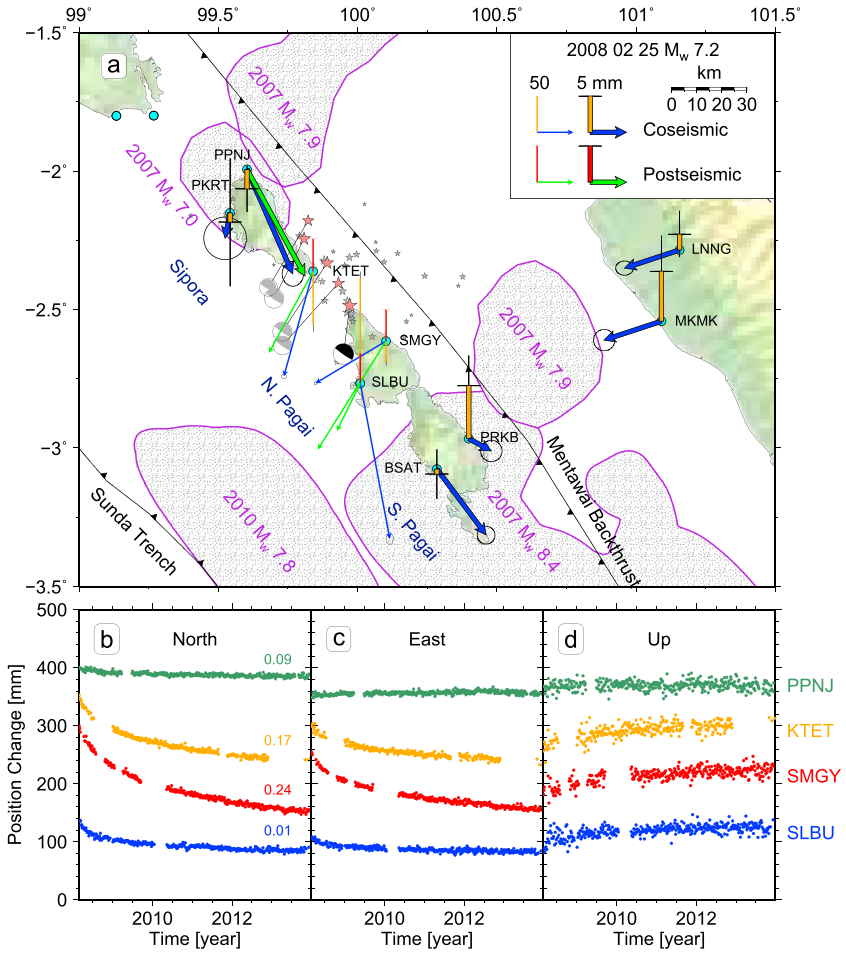

Figure 12. (a) Coseismic and postseismic deformation for the 25 February 2008 M_w 7.2 North Pagai earthquake. Coseismic offsets and postseismic displacements up to the end of 2013 are from this study. Focal mechanisms from gCMT for the main shock and the one M_w 6.5 foreshock and three $M \geq 6$ aftershocks are in black and gray, respectively. Stars denote ANSS earthquakes that occurred within 20 days from 19 February 2008, with pink stars representing the five largest events in this sequence. (b–d) Postseismic time series for the North Pagai earthquake. See Figure 5 for similar captions.

horizontal motion up to ~28 cm and subsidence up to ~4 cm on the island of Simeulue (Figure 10). The static GPS displacements were particularly sensitive to the fault strike orientation and showed a strong preference for the WNW trending faults [*Hill et al.*, 2015].

All the SuGAr stations north of the equator recorded clear postseismic transients after the 2012 earthquakes (Figure 10). Most of them moved northeastward both coseismically and postseismically. The Simeulue stations (LEWK, BNON, and BSIM) reversed their coseismic subsidence to postseismic uplift, while the stations near the equator (HNKO, BTHL, PSMK, PTLO, and BTET) changed from nearly no coseismic vertical motion to postseismic subsidence. The stations near the equator were in a transition zone with small postseismic deformation, and thus, the postseismic signals became difficult to detect with data of less than 2 years. We therefore remain cautious about the magnitude of the subsidence; however, the subsidence itself seems to be real based on the current data. The postseismic deformation of the 2012 earthquakes provides a rare opportunity to investigate the frictional and viscoelastic responses of the oceanic lithosphere.

4.2. Large Earthquakes

4.2.1. The 2008 M_w 7.4 Simeulue Earthquake, the 2010 M_w 7.8 Banyak Islands Earthquake, and the 2010 M_w 7.2 Simeulue Earthquake

Three large ($7 \leq M < 8$) megathrust earthquakes north of the equator were recorded in our catalog. The earliest event was the 20 February 2008 M_w 7.4 Simeulue earthquake that occurred directly beneath Simeulue

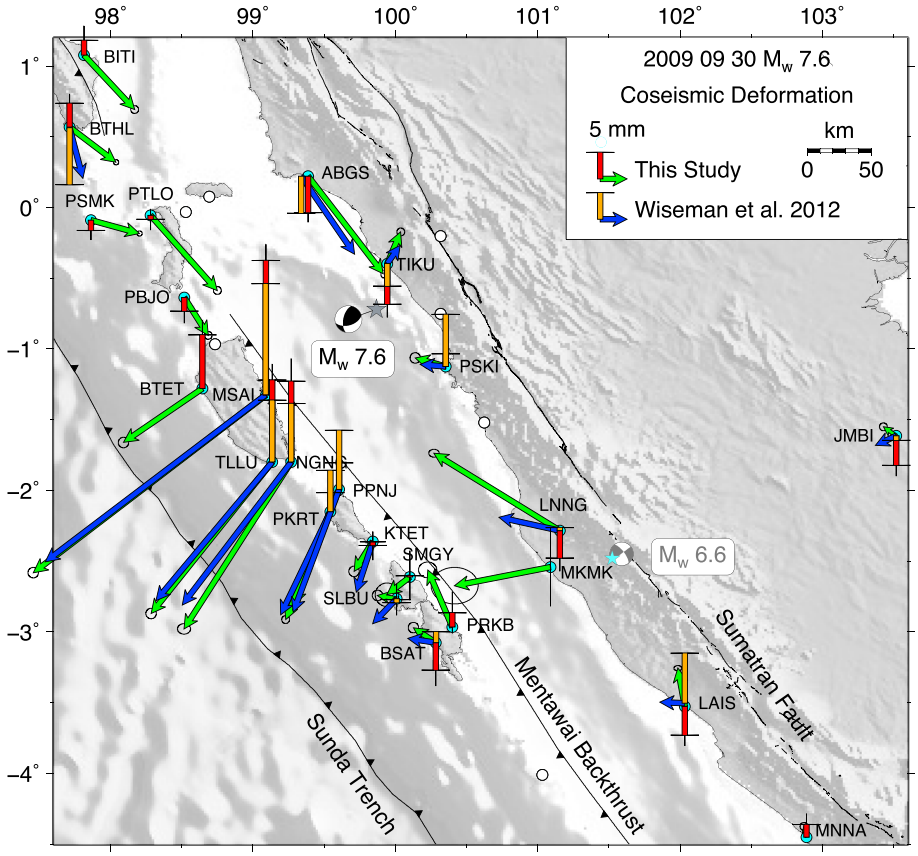

Figure 13. Coseismic deformation for the 30 September 2009 M_w 7.6 Padang earthquake. See Figure 4 for similar captions.

and uplifted a large portion of Simeulue. The uplift pattern was well documented by coral microatolls, together with two SuGAr stations (Figure 11b). Around the same area, another M_w 7.4 earthquake occurred on 2 November 2002 [*DeShon et al.*, 2005]; however, the uplift pattern of this earlier event was documented only by coral microatolls. The coral uplift pattern of the two earthquakes differed appreciably, suggesting the rupture patches were not identical but closely spaced [*Meltzner et al.*, 2010, 2012]. Nevertheless, the two earthquakes both occurred within the Simeulue Saddle, where minimal slip occurred during the great 2004 and 2005 earthquakes.

The other two events occurred in 2010 only 1 month apart. First, the 6 April M_w 7.8 Banyak Islands earthquake occurred near the low-slip region of the 2005 Nias-Simeulue coseismic rupture (Figure 11c). Second, the 9 May M_w 7.2 Simeulue earthquake occurred near the southern terminus of the 2004 Sumatra-Andaman rupture (Figure 11a). Coseismic displacements were recorded at several stations for the two 2010 events with the largest at PBLI for the April event and at LEWK for the May event.

All three of these events generated detectable postseismic deformation recorded by one or more stations (Figures 11d–11f). The 2008 M_w 7.4 and 2010 M_w 7.2 events had similar logarithmic decay times of several weeks, while the largest event had three scales of decay times from several days, several months, to about 1 year. The relative importance of poroelastic, afterslip, and viscoelastic effects is still largely unknown.

GPS observations for these three earthquakes have never been published elsewhere; thus, our results provide new information about the location, slip distribution, and postseismic process of these earthquakes.

4.2.2. The 2008 M_w 7.2 North Pagai Earthquake

The 25 February 2008 M_w 7.2 North Pagai earthquake occurred in a patch with no slip between the northern and southern coseismic slip patches of the 2007 Bengkulu earthquake sequence (Figure 12a). According to the ANSS catalog, the North Pagai earthquake was accompanied by an earthquake sequence that began on 19 February 2008 and lasted for about 20 days. The earthquake sequence included one M_w 6.5

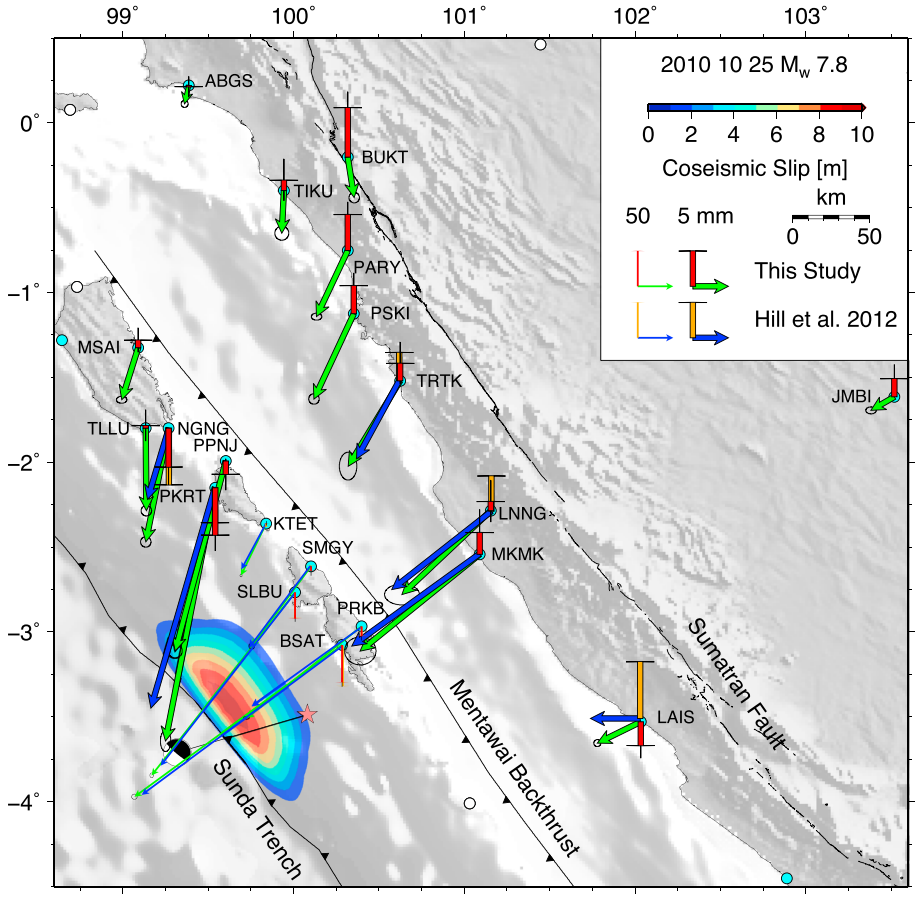

Figure 14. Coseismic deformation for the 25 October 2010 M_w 7.8 Mentawai earthquake. Closed contours show areas of coseismic slip ≥1 m for the Mentawai earthquake [*Hill et al.*, 2012]. See Figure 4 for similar captions.

foreshock and three $M \geq 6$ aftershocks, two of them on the same day as the North Pagai earthquake. This sequence was recorded by an onland temporary seismic array deployed between December 2007 and October 2008 [*Collings et al.*, 2012]. Using these local seismic data, *Collings et al.* [2012] showed that the North Pagai earthquake and its aftershocks occurred on the slab interface.

Our results, as the first GPS observations published for this event, show that nine SuGAr stations moved trenchward during this earthquake, confirming the megathrust origin (Figure 12a). In addition, four SuGAr stations (PPNJ, KTET, SMGY, and SLBU) recorded clear postseismic transients (Figures 12b–12d).

4.2.3. The 2009 M_w 7.6 Padang Earthquake

The 2009 M_w 7.6 Padang earthquake was a deep (~80 km) intraslab event that appears to have occurred within the lower part of the subducting slab and may have even penetrated into the mantle part of the slab [*McCloskey et al.*, 2010; *Wiseman et al.*, 2012]. The focal mechanism rotated to the local dip of the slab indicated a slightly oblique strike-slip event, with either right-lateral motion along an E-W plane or left-lateral motion along a N-S plane [*McCloskey et al.*, 2010]. Neither seismic data nor GPS data could resolve the nodal plane ambiguity, while aftershock activity was more closely aligned with the E-W plane [*McCloskey et al.*, 2010; *Wiseman et al.*, 2012]. No postseismic transients could be found in the SuGAr data for this earthquake [this study; *Wiseman et al.*, 2012], making it the only $M \geq 7$ earthquake that did not generate any detectable postseismic signals.

Compared with megathrust earthquakes, the 2009 Padang earthquake produced coseismic deformation in a much wider area with respect to its magnitude. The affected area extended ~800 km along strike from BITI to MNNA (Figure 13). However, the deformation gradient was much smaller than that of megathrust earthquakes. Using the epicenter as the origin, horizontal motions toward the epicenter were recorded by stations in the northwest and southeast quadrants, while horizontal motions away from the epicenter were recorded

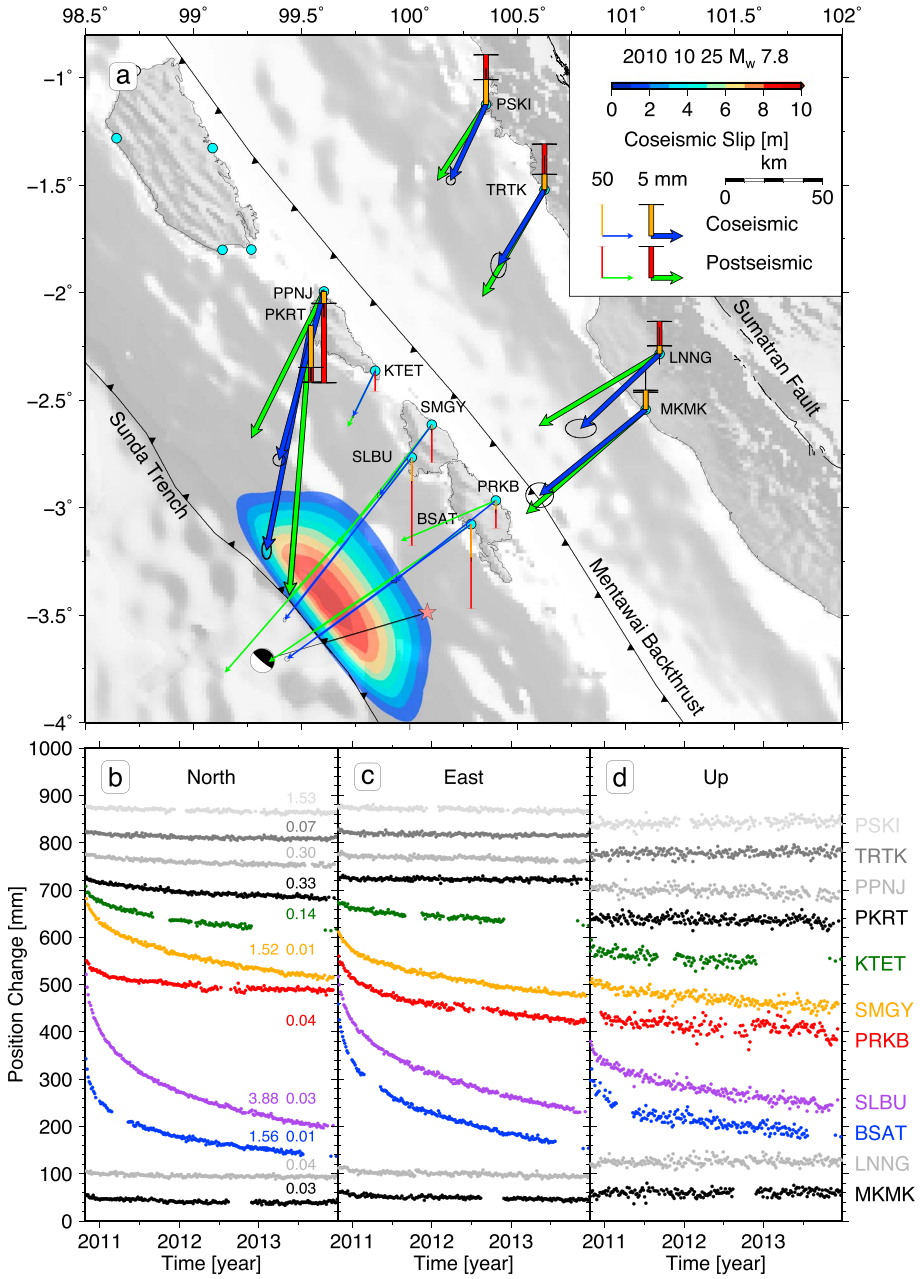

Figure 15. (a) Coseismic and postseismic deformation for the 25 October 2010 M_w 7.8 Mentawai earthquake. Coseismic offsets and postseismic displacements up to the end of 2013 are from this study. (b–d) Postseismic time series for the Mentawai earthquake. See Figure 5 for similar captions.

by stations in the southwest and northeast quadrants. This pattern of horizontal deformation was consistent with the strike-slip focal solution, while vertical motions were uplift at most island stations and subsidence at most coastal stations.

Our coseismic offsets generally agree well with those published by *Wiseman et al.* [2012], but we include eight more SuGAr stations, mainly in the northwest and southeast quadrants (Figure 13). With these additional stations, resolving the nodal plane ambiguity might become possible.

Two stations (LNNG and MKMK) exhibited unusually large displacements (Figure 13). These large displacements were caused by a M_w 6.6 strike-slip event on the Sumatran fault that occurred about 16 h after the Padang earthquake. Thus, if the daily solutions are used, the coseismic deformation field of the Padang earth-

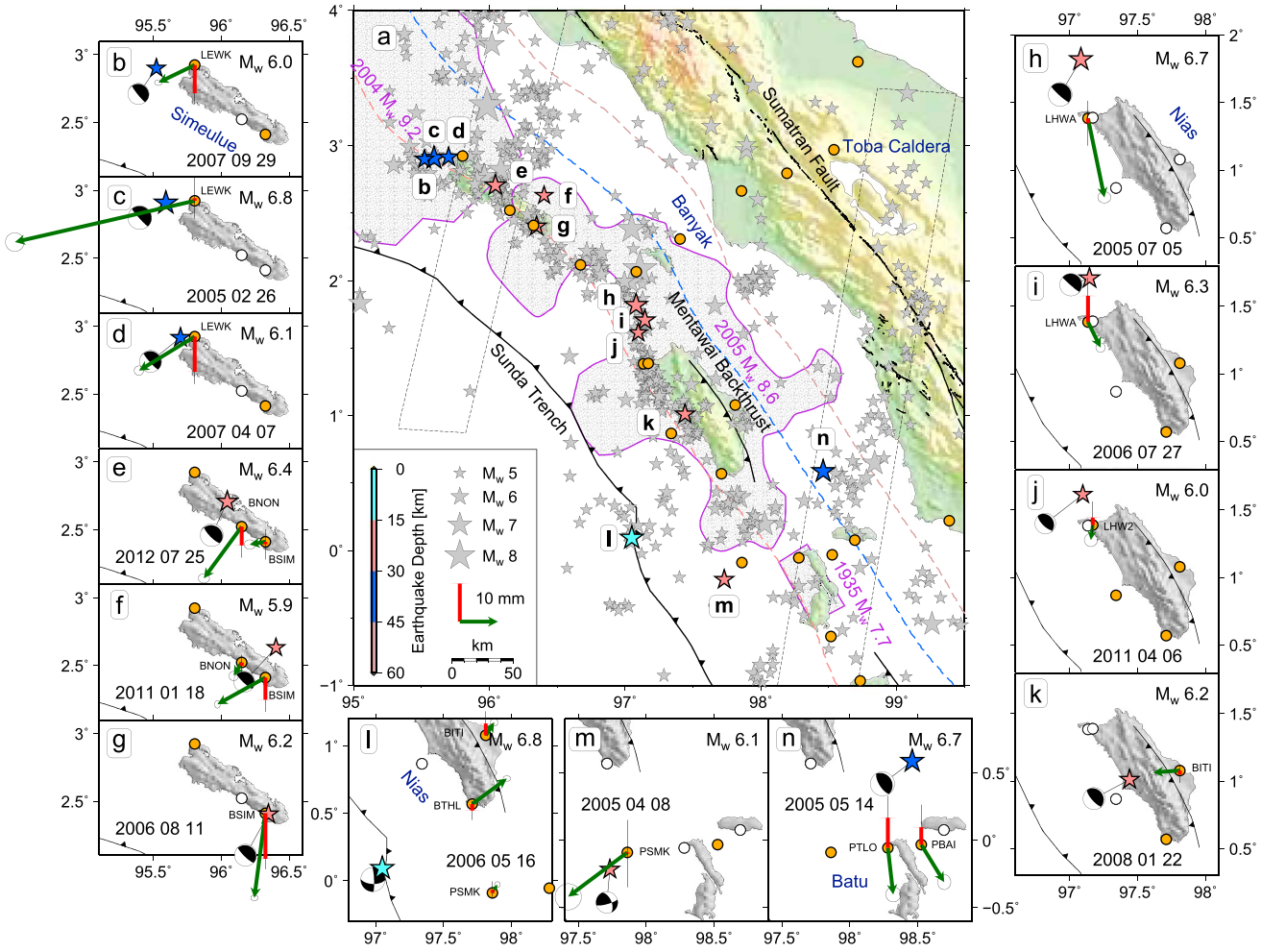

Figure 16. Thirteen moderate earthquakes with magnitudes in the range of 5.9–6.8 recorded by the SuGAr at the equator or north of the equator. (a) Stars colored by hypocenter depth indicate earthquakes with deformation recorded by the SuGAr. Gray stars represent $M \geq 5$ earthquakes from 1963 to 2013 in the ANSS catalog. Shaded patches outline the main slip areas of the 2004 Sumatra-Andaman and 2005 Nias-Simeulue earthquakes and the estimated rupture location of the 1935 M_w 7.7 Batu earthquake [*Rivera et al.*, 2002]. Black dashed boxes delineate the inferred subducted fracture zones underneath Simeulue [*Franke et al.*, 2008] and Batu Islands [*Pesicek et al.*, 2010] based on seismicity. Orange circles denote SuGAr stations. (b–n) Coseismic offsets recorded at SuGAr stations for each of the 13 earthquakes, individually, using the same map and vector scales. Error ellipses represent 95% confidence levels. Orange and white circles are active and inactive stations during the event.

quake would have been influenced by this strike-slip event, in particular, at LNNG, MKMK, LAIS, MNNA, and JMBI. *Wiseman et al.* [2012] removed coseismic offsets associated with this M_w 6.6 earthquake for LNNG; however, they did not report values for any other affected stations.

4.2.4. The 2010 M_w 7.8 Mentawai Earthquake

The 2010 M_w 7.8 Mentawai earthquake was classified as a tsunami earthquake, because it produced an anomalously large tsunami compared to its magnitude [*Newman et al.*, 2011; *Lay et al.*, 2011; *Bilek et al.*, 2011; *Hill et al.*, 2012; *Satake et al.*, 2012; *Yue et al.*, 2014]. The coseismic rupture of this event occurred along a near-trench portion of the Sumatran megathrust west of the Mentawai Islands [*Hill et al.*, 2012; *Yue et al.*, 2014]. This event was so shallow that the majority of the coseismic slip concentrated at depths of <6 km, an area of the megathrust previously thought to be creeping and not capable of generating large slips [*Hill et al.*, 2012].

In general, our daily static coseismic displacements are consistent with those from *Hill et al.* [2012]; however, we provide eight more SuGAr estimates in the far field (Figure 14). The horizontal coseismic motions show a systematic convergence toward the main slip area. Coseismic subsidence was observed at most island stations with the maximum of ~5.3 cm recorded at BSAT. In contrast, a small coseismic uplift of ≤0.7 mm was observed at most coastal stations except at LAIS.

These daily static coseismic displacements were considerably larger than the 1 s high-rate kinematic solutions [*Hill et al.*, 2012]. This discrepancy suggests that a large amount of postseismic displacement occurred rapidly within the first day of the earthquake. We identified clear postseismic deformation recorded by 11 SuGAr stations (Figure 15). The postseismic displacements of almost all these 11 stations had exceeded their coseismic displacements by the end of 2013. In particular, the vertical postseismic displacements at many sites were several times larger than the coseismic displacements.

4.3. Moderate Earthquakes

4.3.1. Northern Moderate Earthquakes

Thirteen moderate earthquakes with magnitudes ranging from 5.9 to 6.8 were recorded by the SuGAr at the equator or north of the equator. None of these 13 moderate earthquakes have been studied using GPS before. They created horizontal displacements of several millimeters to several centimeters and vertical displacements of less than 1 cm at the SuGAr stations.

Of these, 10 were thrust earthquakes that occurred within a narrow curved seismic band along the trench-side coastlines of Simeulue and Nias (Figure 16a). This curved seismic band became active mainly after the 2005 Nias-Simeulue earthquake [*Pesicek et al.*, 2010], with most earthquakes within the band being shallowly dipping thrust events on the megathrust [*Tilmann et al.*, 2010]. The ANSS seismicity locations in this band approximately follow the 20 km depth slab contour, passing beneath Simeulue and immediately west of Nias (Figure 16a); however, these teleseismic locations have relatively large uncertainties that can be up to tens of kilometers horizontally [*Dewey et al.*, 2007; *Tilmann et al.*, 2010]. Our near-field GPS observations provide independent information about the locations. We find coseismic subsidence of Simeulue during five events (Figures 16b and 16d–16g), suggesting these five moderate ruptures occurred seaward of Simeulue. This is similar to what *Tilmann et al.* [2010] found for local seismicity, which was absent beneath Simeulue but concentrated seaward of Simeulue [Figure 2 in *Tilmann et al.*, 2010].

The 14 May 2005 M_w 6.7 event occurred at the boundary of a NNE-SSW trending linear seismic band which extends and deepens from north of the Batu Islands to north of Toba Caldera (Figure 16a). This linear seismic band is less pronounced in the ANSS catalog as shown in Figure 16a but has been well imaged by both local earthquake locations and teleseismic double-difference relocation and inferred to reflect the subducted prolongation of the Investigator Fracture Zone (IFZ) [*Fauzi et al.*, 1996; *Lange et al.*, 2010; *Pesicek et al.*, 2010]. The nature of seismicity along the subducted IFZ is currently unknown using available focal mechanism solutions [*Pesicek et al.*, 2010]. The 14 May 2005 event had a thrust focal mechanism with a depth of 39 (gCMT) or 34 km (ANSS). These seismological observations cannot distinguish between the two ambiguous focal planes; however, the southsoutheastward and upward motions of PTLO and PBAI suggest this event more likely to be a megathrust earthquake (Figure 16n). Although the ANSS location appears to be inside the IFZ, it is also possible that this event was on an undisrupted megathrust patch immediately northwest of where the IFZ disrupts the megathrust.

The 8 April 2005 M_w 6.1 event occurred near the southern promontory of the 2005 Nias-Simeulue rupture only 1 week after the 2005 earthquake (Figure 16a). This event was a strike-slip event with a depth of 12 (gCMT) or 20.9 km (ANSS). According to the southwestward motion of PSMK (Figure 16m), this event is a left-lateral strike-slip earthquake. However, we cannot distinguish whether this event was within the overlying accretionary wedge, the uppermost part of the slab, or the subducting oceanic crust. Nevertheless, its close relationship in space and time to the 2005 earthquake and the left-lateral mechanism on a NE-SW trending plane suggest this M_w 6.1 event was possibly a result of strain relaxation at the boundary of the 2005 rupture.

The 16 May 2006 M_w 6.8 event occurred very close to the Sunda trench at a shallow depth, representing a cluster of similar strike-slip events (Figure 16a). It is difficult to distinguish whether this event occurred in the outer rise of the subducting plate or in the accretionary wedge of the overriding plate. In either case, this event probably occurred in response to some preexisting oceanic plate fabric that is or close to being subducted. Outboard of the trench in the Wharton Basin, where the oceanic seafloor has not been subducted, the most prominent fabrics are N-S trending fracture zones and E-W trending ridge segments of the fossil Wharton spreading center [*Deplus et al.*, 1998; *Jacob et al.*, 2014]. Some of the N-S trending fracture zones have been locally reactivated as left-lateral strike-slip faults [*Deplus et al.*, 1998; *Graindorge et al.*, 2008]; meanwhile, active deformation along the near-conjugate E-W trending planes has also been suggested by the 2000 M_w 7.8 Wharton Basin earthquake [*Robinson et al.*, 2001], and most recently by the 2012 M_w 8.6 and 8.2 Wharton Basin earthquakes (section 4.1.4). Unfortunately, for this M_w 6.8 event, only one SuGAr station (BTHL) recorded large

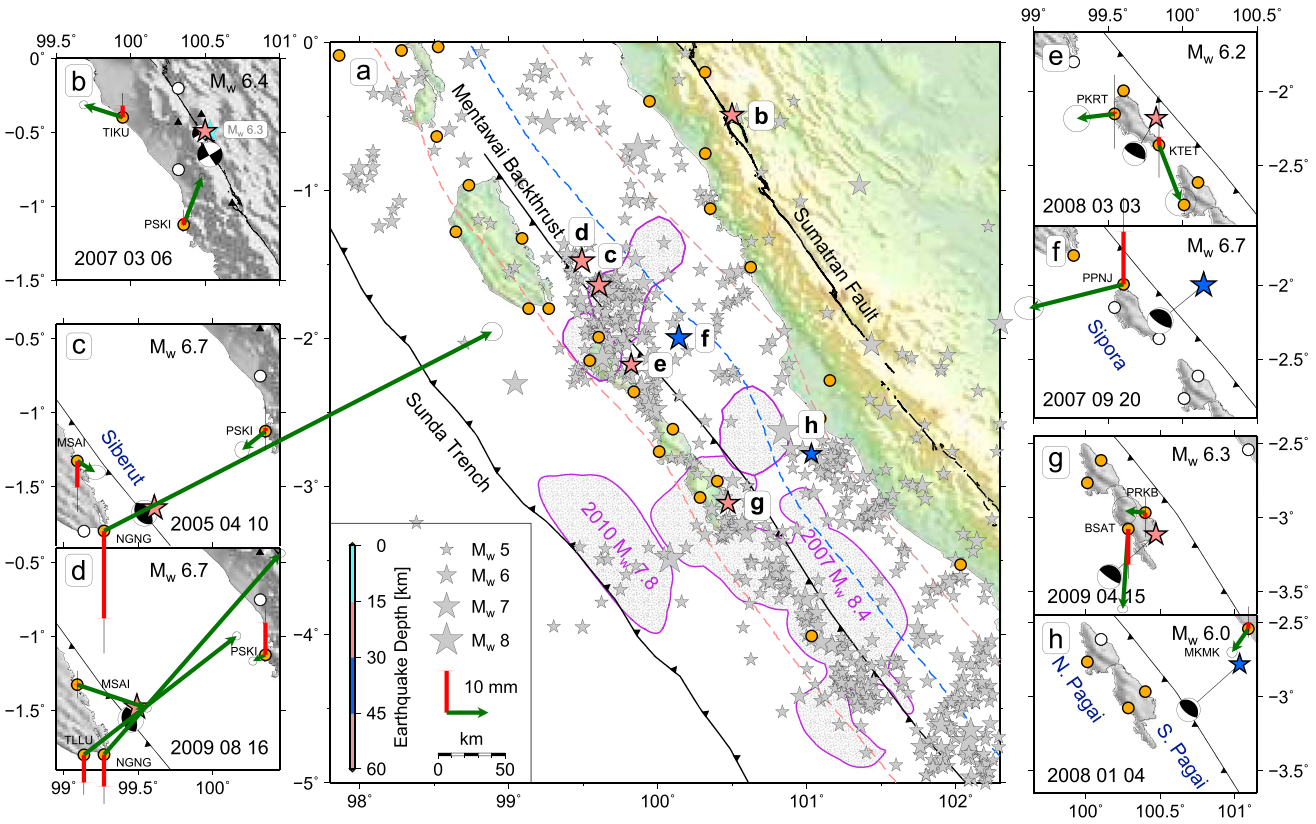

Figure 17. (a–h) Seven moderate earthquakes with magnitudes in the range of 6.0– 6.7 recorded by the SuGAr south of the equator. See Figure 16 for similar captions.

enough displacement; its northeastward horizontal motion is too equivocal to distinguish which of the two planes was active during this event (Figure 16l).

4.3.2. Southern Moderate Earthquakes

Seven moderate earthquakes with magnitudes in the range of 6.0–6.7 were recorded by the SuGAr south of the equator. Among these seven moderate earthquakes, to the best of our knowledge, only the 10 April 2005 and 16 August 2009 M_w 6.7 back thrust earthquakes have been studied before [*Wiseman et al.*, 2011]. Compared to the northern moderate earthquakes, even though the southern moderate earthquakes have a smaller range of magnitudes, they have larger variations in displacements.

The 6 March 2007 M_w 6.4 event and 2 h later another M_w 6.3 earthquake occurred along two adjacent segments of the Sumatran fault near Padang [*Nakano et al.*, 2010; *Daryono et al.*, 2012]. This 2007 doublet was not the first one in this section; doublets have repeatedly occurred in 1926, in 1943, and perhaps in 1822 [*Untung et al.*, 1985; *Sieh and Natawidjaja*, 2000; *Prawirodirdjo et al.*, 2000; *Daryono et al.*, 2012]. The surface ruptures of the two events, as mapped in the field, had average total offsets of 56 and 40 cm, respectively, with some vertical motion [*Daryono et al.*, 2012]. Two SuGAr stations (TIKU and PSKI) recorded the combined effect of this doublet with ~1 cm horizontal and little vertical displacement (Figure 17b).

The 10 April 2005 M_w 6.7 and 16 August 2009 M_w 6.7 events occurred close to each other immediately east of southern Siberut (Figure 18a). They distinguished themselves by unusual large landward horizontal coseismic motions (Figures 17c and 17d). This deformation pattern can be only reasonably explained by a back thrust on the Mentawai fault [*Wiseman et al.*, 2011]. Whether the Mentawai fault is mainly a strike-slip or thrust fault was previously in high debate [e.g., *Diament et al.*, 1992; *Malod and Kemal*, 1996; *Samuel and Harbury*, 1996; *Sieh and Natawidjaja*, 2000]. However, these two recent earthquakes provide strong support for the Mentawai fault to be an active back thrust [*Wiseman et al.*, 2011].

These two earthquakes were the main shocks in two back thrust earthquake sequence. The 2005 sequence started gradually after the 2005 Nias-Simeulue earthquake and accumulated to an equivalent M_w 6.9 earth-

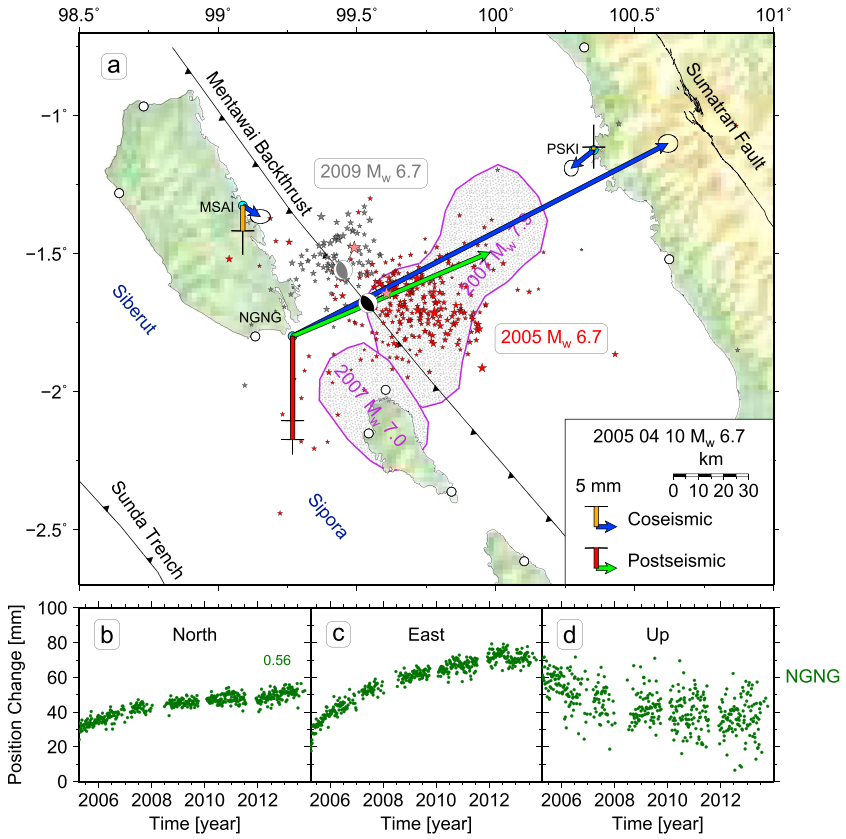

Figure 18. (a) Coseismic and postseismic deformation for the 10 April 2005 M_w 6.7 back thrust earthquakes. Coseismic offsets and postseismic displacements up to the end of 2013 are from this study. Shaded patches outline two main slip areas of the M_w 7.9 and M_w 7.0 aftershocks following the 2007 Bengkulu earthquake. Red and gray stars denote ANSS earthquakes in April 2005 and from 16 August 2009 to 15 September 2009, respectively. (b–d) NGNG postseismic time series for the 2005 back thrust event. See Figure 5 for similar captions.

quake between 2 April 2005 and 17 April 2005 [*Wiseman et al.*, 2011]. The 10 April 2005 event even generated a local tsunami up to 1 m high on the southeastern coast of Siberut [*Wiseman et al.*, 2011]. The 2009 sequence began with the largest event on 16 August 2009 just north of the 2005 sequence and lasted only 1 week with much less seismicity than the 2005 sequence, which amounts to a M_w 6.7 earthquake [*Wiseman et al.*, 2011]. The reported depths of the 2009 sequence were ~10 km, much shallower than the ~30 km depths of the 2005 sequence.

We find a small but clear postseismic transient at NGNG associated with the 2005 back thrust sequence (Figures 18b–18d). Due to this sequence, NGNG has accumulated postseismic horizontal motion of ~5 cm and vertical motion of ~2.5 cm by the end of 2013. Initially, we attributed this signal to the M_w 8.6 Nias-Simeulue earthquake. However, we excluded this possibility based on the following reasons. First, the 10 April 2005 back thrust event coseismically generated 10 cm landward horizontal motion and 2 cm subsidence at NGNG (Figure 18a), while the Nias-Simeulue earthquake only generated 1 cm southeastward motion and almost no vertical motion (Figure 6). Although the Nias-Simeulue earthquake was 19 times larger than the back thrust event, the back thrust event created 10 times larger deformation at NGNG locally. Second, the eastward postseismic motion could not fit into the postseismic deformation field of the Nias-Simeulue earthquake (Figures 7a and 18a). Third, the postseismic motion at NGNG was larger than at two stations (MSAI and PSKI) closer to the Nias-Simeulue rupture. We did not find any obvious postseismic signals that can be associated with the 2009 sequence. It seems like the 2009 sequence was not energetic enough to trigger detectable postseismic deformation. The observable postseismic deformation may be attributed to the additional 0.2 moment magnitude of the 2005 sequence compared to the 2009 sequence.

The 20 September 2007 M_w 6.7 event occurred beneath the fore-arc basin between Sipora and the west coast of Sumatra about a week after the 2007 M_w 8.4 Bengkulu earthquake. The 3 March 2008 M_w 6.2 event occurred

just east of Sipora also about a week after the 2008 M_w 7.2 event. Seaward horizontal motions (Figures 17e and 17f), together with the timing, focal plane solutions, and focal depths, indicate that these two events were triggered aftershocks on the plate interface. Interestingly, the 20 September 2007 event generated >1 cm uplift at PPNJ (Figure 17f), while the 3 March 2008 event produced little uplift at KTET and PKRT (Figure 17e). The location of the 3 March 2008 rupture was likely just beneath Sipora, while the location of the 20 September 2007 rupture was probably deeper than the location of the 3 March 2008 rupture.

The 15 April 2009 M_w 6.3 event occurred near the southern end of South Pagai (Figure 17a), where a local maximum of uplift was documented during the 2007 Bengkulu earthquake. This event was a thrust event with a depth of 15 (gCMT) or 22 km (ANSS). This event could be a thrust earthquake on the megathrust or on a splay fault within the fore arc. The trenchward motions of BSAT and PRKB can rule out the possibility of this event being a back thrust event (Figure 17g). If we combine the evidence from focal mechanisms, this event was most likely on the megathrust. BSAT recorded subsidence of 8.5 mm, while PRKB recorded little subsidence (Figure 17g), suggesting the rupture patch was seaward of South Pagai. If this event indeed took place on the megathrust seaward of South Pagai, the rupture patch would coincide with one of the high-slip areas in the 2007 coseismic slip models (Figure 8). Such coincidence would suggest some patches within a large rupture could hold off during the main earthquake and fail at a later time.

The 4 January 2008 M_w 6.0 event occurred close to the west coast of Sumatra (Figure 17a). This event was a thrust event with a depth of 46.1 (gCMT) or 35 km (ANSS). MKMK recorded a small seaward horizontal motion and a negligible vertical motion (Figure 17h). We infer that the event could be on the deeper portion of the megathrust or on a reverse fault within the overriding plate.

5. Discussion

5.1. Earthquake Detection Performance

The smallest event in our catalog was a M_w 5.9 event. During the observation period from 5 August 2002 to 31 December 2013, the ANSS catalog documented a total of 141 earthquakes with magnitudes ≥5.9 in the broad Sumatran plate boundary region (gray stars in Figure 3). However, among the 141 events, the SuGAr network recorded only 30 with a detection rate of 21%. Most of the undetected events were too far away from an active GPS station to be recorded (Figure 19). Some of the undetected earthquakes had large magnitudes and were close enough to active stations, but they could not be separately cataloged because they were shadow events that occurred too close to another larger event in time for our daily solutions (Table S1).

Figure 19 shows the detection performance of the SuGAr network based on the relationship between magnitude and station-epicenter distance. Although the epicenter locations could be shifted horizontally by up to tens of kilometers [*Dewey et al.*, 2007; *Tilmann et al.*, 2010], one can still use Figure 19 to roughly estimate within what distance deformation can be expected for a certain magnitude. However, one has to bear in mind other factors, such as focal mechanism, earthquake depth, rupture area, and azimuth of stations with respect to rupture patches.

5.2. Logarithmic Decay Times

In total, our catalog records 72 first (or single) and 18 second logarithmic decay times. The smallest decay time is 0.001 year (half a day) obtained for the postseismic deformation of LEWK associated with the 2005 Nias-Simeulue earthquake. This extremely short decay time is likely an outlier biased by other earthquakes, because LEWK recorded not only the 2004 Sumatra-Andaman earthquake but also a M_w 6.8 event within 3 months prior to the 2005 earthquake. Excluding this outlier, the smallest decay time is 1 day obtained for cases where a second decay is included. For cases where a single decay is used, the smallest decay time is 2–3 days. The largest decay time is 21 years obtained for the postseismic deformation of SAMP, which was probably affected by both the 2004 Sumatra-Andaman and 2005 Nias-Simeulue earthquakes (section 4.1.2). In summary, the logarithmic decay times span a wide range from several days to more than 20 years. Such a wide range of decay times and the need for a second decay time are likely due to different postseismic mechanisms. Even for one earthquake, decay times also vary largely between stations, suggesting that contributions from different postseismic mechanisms need to be assessed before we can safely neglect any of them.

In order to test whether the difference in postseismic decay time can be related to the difference in some earthquake parameters, we searched the statistics of our database for relationships of decay time with

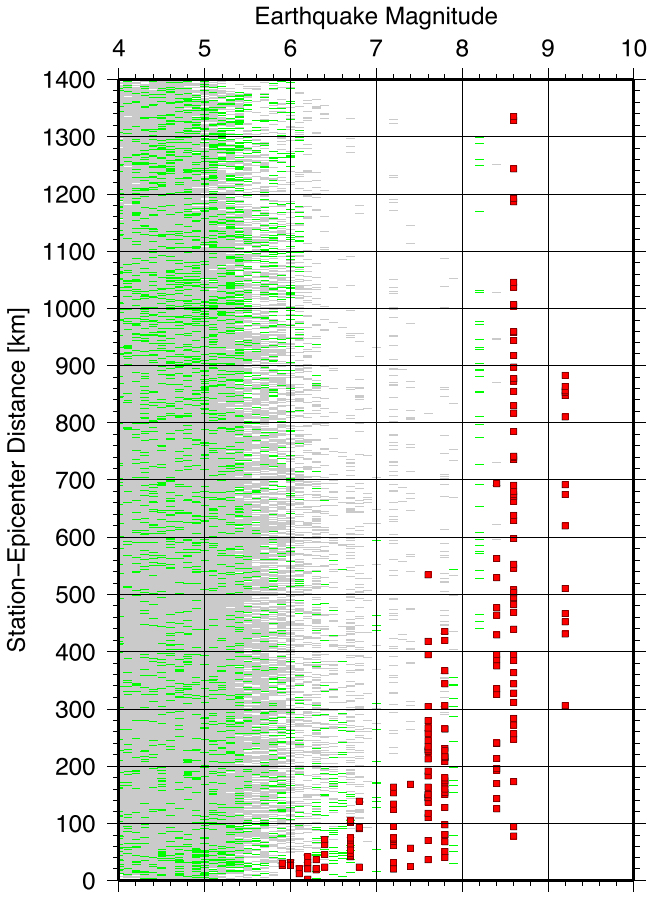

Figure 19. Earthquake magnitude versus station-epicenter distance for pairs of the 39 stations and earthquakes in the broad Sumatran plate boundary region (defined in Figure 1) during the observation period from 5 August 2002 to 31 December 2013. Red squares represent pairs associated with the 39 cataloged earthquakes. Thin green bars indicate pairs associated with the undetected earthquakes that occurred within 5 days of a bigger cataloged earthquake, while thin gray bars indicate pairs associated with the rest of the undetected earthquakes. Magnitudes and epicenter locations are from the ANSS catalog.

earthquake magnitude, length of postseismic time series, hypocenter depth, centroid depth, station-epicenter distance, and station-centroid distance (Figure 20).

We find some correlation between earthquake magnitude and decay time (Figure 20a). Smaller earthquakes tend to have a narrower range of decay times, while larger earthquakes tend to have a wider range and a long second decay time. However, this correlation might be related to the fact that one decay time is usually sufficient for relatively small earthquakes, while two different decay times are often required for large earthquakes ($M \geq 7.8$).

We find no clear correlations for decay time with the other parameters that we tested (Figures 20b–20f). One explanation for no clear correlations is that there is genuinely no difference in the postseismic response to earthquakes of different depths or along-strike locations, but this seems contrary to our expectation for a greater level of viscoelastic deformation from, for example, earthquakes nucleating at greater depths. Another explanation is that this is simply a sampling issue, and to identify any pattern or correlation will require more stations and even longer records. Alternatively, a pattern or correlation may exist for signals that are solely related to one postseismic mechanism, for example, afterslip or viscoelastic relaxation. The lack of a clear pattern or correlation could reflect remaining difficulties in separating the signals of afterslip from viscoelastic deformation. We thus remain cautious about our results showing no correlation for the different decay times in that the postseismic processes are possibly affected by multiple variables that may not be easy to quantify.

5.3. Postseismic Velocity Time Series

Our catalog documents a total of 72 postseismic displacement time series that have seasonal signals, long-term rates, offsets, and postseismic decays of all other earthquakes removed. By calculating the gradient of the fits to these 72 postseismic displacement time series, we derived postseismic velocity time series (Figure 21). In general, the postseismic velocity is high in the first few months after an earthquake and gradually decays to nearly zero (within the data noise) over the next few years or tens of years. In the beginning of the postseismic process, the postseismic velocity could be as high as 4–6 m/yr for horizontal and 1–2 m/yr for vertical; after 5 years, the postseismic velocity normally decreases to less than 3 cm/yr for horizontal (Figure 21a) and less than 1 cm/yr for vertical (Figure 21b). How fast the postseismic velocity decays likely depends on the magnitude of the earthquake. After the 2005 M_w 6.7 moderate earthquake, it took NGNG only about 2 years to reach a millimeter per year velocity level (the single red line in Figures 21a and 21b); however, after the 2004 M_w 9.2 great Sumatra-Andaman earthquake, UMLH gradually accelerated to an uplift rate of ~3 cm/yr within 1 year, and since then, it has been uplifting at a rate of ~3 cm/yr and has not shown any sign of slowing down (section 4.1.1). Such high postseismic velocity after a decade of the earthquake demonstrates how

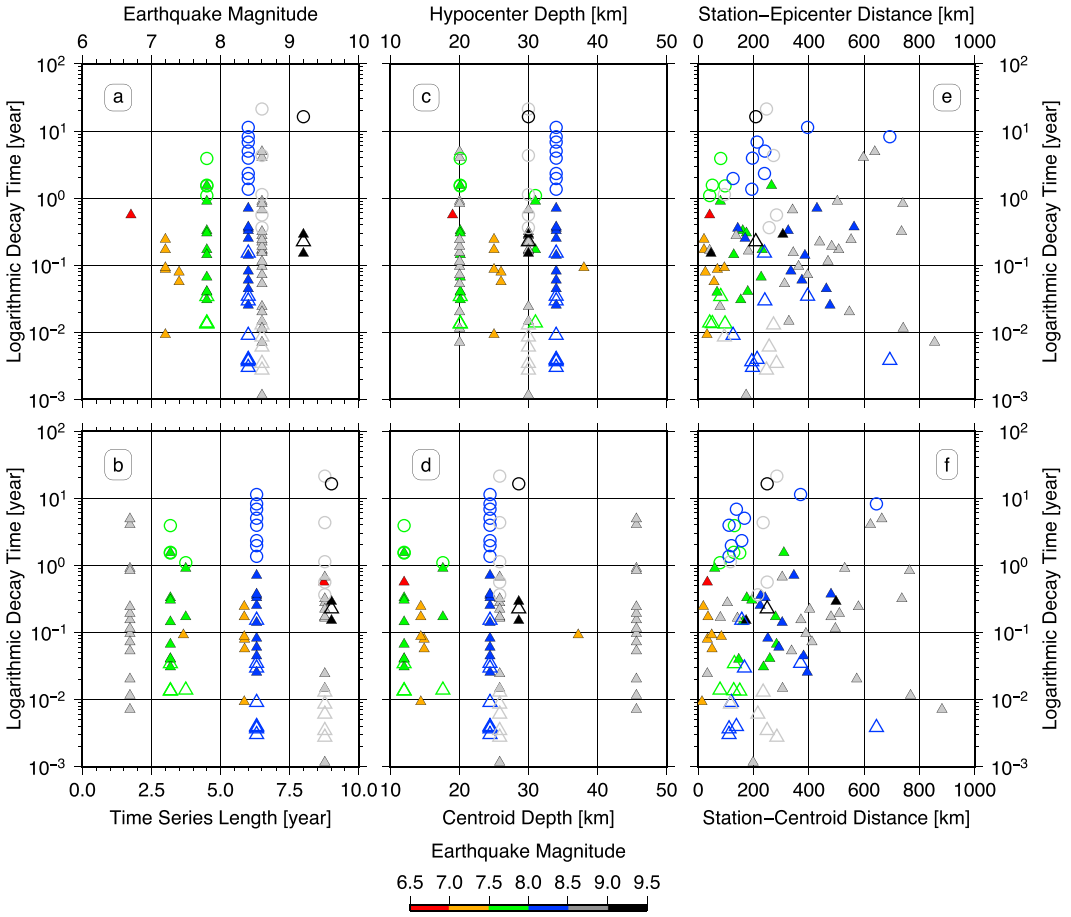

Figure 20. Relationships of postseismic logarithmic decay time with (a) earthquake magnitude, (b) length of postseismic time series, (c) ANSS hypocenter depth, (d) gCMT centroid depth, (e) ANSS station-epicenter distance, and (f) gCMT station-centroid distance. Solid triangles, hollow triangles, and hollow circles represent the single, first shorter, and second longer logarithmic decay times, respectively. Symbol colors indicate earthquake magnitude.

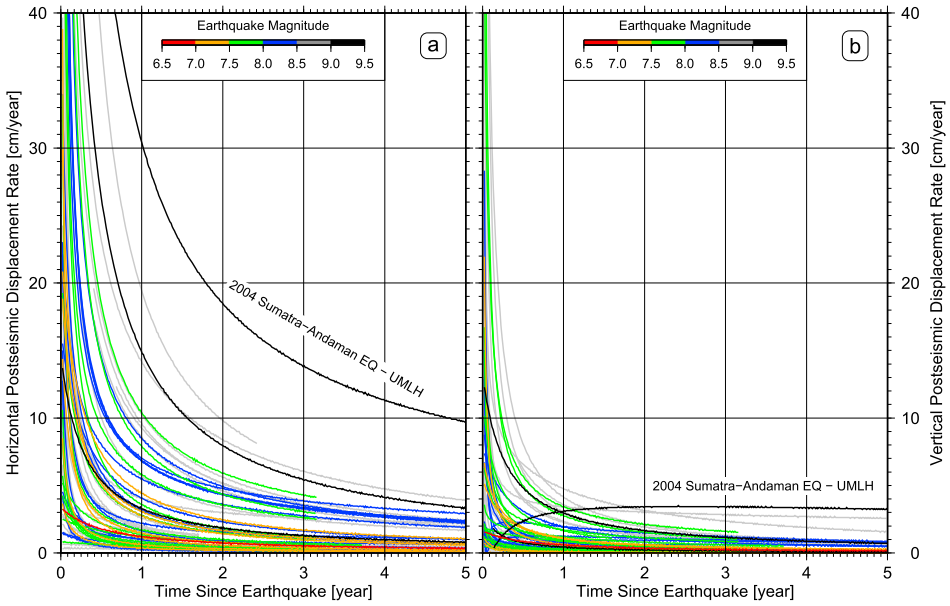

Figure 21. (a) Horizontal postseismic velocity time series. (b) Vertical postseismic velocity time series. Curve colors indicate earthquake magnitude.

interseismic rates can be modulated by postseismic displacements and highlights the difficulty in separating them when records are not long enough.

6. Conclusion

In this paper, we have produced the first GPS-based earthquake catalog for the Sumatran plate boundary from August 2002 to the end of 2013. We have shown that our catalog is a comprehensive and useful resource for studying the Sumatran plate boundary and its earthquakes. This catalog is so rich that it likely asks more questions than it answers. We hope this catalog and the accompanied supporting information tables will enable more careful and comprehensive modeling studies and provide fuel for a wealth of exciting new research in the future.

Acknowledgments

The SuGAr daily RINEX files are available for public download at ftp://eos.ntu.edu.sg/SugarData with a latency of 3 months. The complete catalog for the 30 Sumatran earthquakes can be found in the supporting information tables. Figures were made using Generic Mapping Tools [*Wessel et al.*, 2013]. We are very grateful to many scientists and field technicians who helped install and maintain the SuGAr network over the past decade. These include John Galetzka, Jeffrey Encillo, Imam Suprihanto, and Dudi Prayudi. We thank Pedro Elosegui for sharing his experience in GIPSY processing. We thank Sylvain Barbot, Qiang Qiu, and Rino Salman for useful discussions and Aron Meltzner and Jeff Freymueller for comments on the early drafts of this paper. We appreciate the Associate Editor, Roland Bürgmann, and one anonymous reviewer for their constructive and detailed comments that have greatly improved, strengthened, and shortened the paper. We would like to express our special thanks to Pavel Adamek for all his invaluable linguistic suggestions that greatly improved the English writing of this paper.

This research was supported by the National Research Foundation Singapore under its Singapore NRF Fellowship scheme (National Research Fellow Award NRF-NRFF2010-064 to E.M.H.) and by the Earth Observatory of Singapore via its funding from the National Research Foundation Singapore and the Singapore Ministry of Education under the Research Centres of Excellence initiative. This is Earth Observatory of Singapore paper number 79.

References

Altamimi, Z., X. Collilieux, and L. Métivier (2011), ITRF2008: An improved solution of the International Terrestrial Reference Frame, *J. Geod.*, *85*(8), 457–473, doi:10.1007/s00190-011-0444-4.

Altamimi, Z., L. Métivier, and X. Collilieux (2012), ITRF2008 plate motion model, *J. Geophys. Res.*, *117*, B07402, doi:10.1029/2011JB008930.

Aster, R. C., B. Borchers, and C. H. Thurber (2005), *Parameter Estimation and Inverse Problems*, 1st ed., 320 pp., Elsevier Acad. Press, Burlington, Mass.

Banerjee, P., F. F. Pollitz, and R. Bürgmann (2005), The size and duration of the Sumatra-Andaman earthquake from far-field static offsets, *Science*, *308*(5729), 1769–1772, doi:10.1126/science.1113746.

Banerjee, P., F. Pollitz, B. Nagarajan, and R. Bürgmann (2007), Coseismic slip distributions of the 26 December 2004 Sumatra-Andaman and 28 March 2005 Nias earthquakes from GPS static offsets, *Bull. Seismol. Soc. Am.*, *97*(1A), S86–S102, doi:10.1785/0120050609.

Bar-Sever, Y. E., P. M. Kroger, and J. A. Borjesson (1998), Estimating horizontal gradients of tropospheric path delay with a single GPS receiver, *J. Geophys. Res.*, *103*(B3), 5019–5035, doi:10.1029/97JB03534.

Barbot, S., Y. Fialko, and Y. Bock (2009), Postseismic deformation due to the M_w 6.0 2004 Parkfield earthquake: Stress-driven creep on a fault with spatially variable rate-and-state friction parameters, *J. Geophys. Res.*, *114*, B07405, doi:10.1029/2008JB005748.

Bertiger, W., S. D. Desai, B. Haines, N. Harvey, A. W. Moore, S. Owen, and J. P. Weiss (2010), Single receiver phase ambiguity resolution with GPS data, *J. Geod.*, *84*(5), 327–337, doi:10.1007/s00190-010-0371-9.

Bilek, S. L., E. R. Engdahl, H. R. DeShon, and M. El Hariri (2011), The 25 October 2010 Sumatra tsunami earthquake: Slip in a slow patch, *Geophys. Res. Lett.*, *38*, L14306, doi:10.1029/2011GL047864.

Blewitt, G., and D. Lavallée (2002), Effect of annual signals on geodetic velocity, *J. Geophys. Res.*, *107*(B7), 2145, doi:10.1029/2001JB000570.

Boehm, J., B. Werl, and H. Schuh (2006), Troposphere mapping functions for GPS and very long baseline interferometry from European Centre for Medium-Range Weather Forecasts operational analysis data, *J. Geophys. Res.*, *111*, B02406, doi:10.1029/2005JB003629.

Borrero, J. C., R. Weiss, E. A. Okal, R. Hidayat, D. A. Suranto, and V. V. Titov (2009), The tsunami of 2007 September 12, Bengkulu province, Sumatra, Indonesia: Post-tsunami field survey and numerical modelling, *Geophys. J. Int.*, *178*(1), 180–194, doi:10.1111/j.1365-246X.2008.04058.x.

Briggs, R. W., et al. (2006), Deformation and slip along the Sunda megathrust in the great 2005 Nias-Simeulue earthquake, *Science*, *311*, 1897–1901, doi:10.1126/science.1122602.

Bürgmann, R., S. Ergintav, P. Segall, E. H. Hearn, S. McClusky, R. E. Reilinger, H. Woith, and J. Zschau (2002), Time-dependent distributed afterslip on and deep below the Izmit earthquake rupture, *Bull. Seismol. Soc. Am.*, *92*(1), 126–137, doi:10.1785/0120000833.

Chlieh, M., et al. (2007), Coseismic slip and afterslip of the great M_w 9.15 Sumatra-Andaman Earthquake of 2004, *Bull. Seismol. Soc. Am.*, *97*, S152–S173, doi:10.1785/0120050631.

Collings, R., D. Lange, A. Rietbrock, F. Tilmann, D. Natawidjaja, B. Suwargadi, M. Miller, and J. Saul (2012), Structure and seismogenic properties of the Mentawai segment of the Sumatra subduction zone revealed by local earthquake traveltime tomography, *J. Geophys. Res.*, *117*, B01312, doi:10.1029/2011JB008469.

Daryono, M. R., D. H. Natawidjaja, and K. Sieh (2012), Twin-surface ruptures of the March 2007 $M > 6$ earthquake doublet on the Sumatran fault, *Bull. Seismol. Soc. Am.*, *102*(6), 2356–2367, doi:10.1785/0120110220.

DeMets, C., R. G. Gordon, and D. F. Argus (2010), Geologically current plate motions, *Geophys. J. Int.*, *181*(1), 1–80, doi:10.1111/j.1365-246X.2009.04491.x.

Deplus, C., M. Diament, H. Hébert, G. Bertrand, S. Dominguez, J. Dubois, J. Malod, P. Patriat, B. Pontoise, and J.-J. Sibilla (1998), Direct evidence of active deformation in the eastern Indian oceanic plate, *Geology*, *26*(2), 131–134, doi:10.1130/0091-7613(1998)026<0131:DEOADI>2.3.CO;2.

DeShon, H. R., E. R. Engdahl, C. H. Thurber, and M. Brudzinski (2005), Constraining the boundary between the Sunda and Andaman subduction systems: Evidence from the 2002 M_w 7.3 Northern Sumatra earthquake and aftershock relocations of the 2004 and 2005 great earthquakes, *Geophys. Res. Lett.*, *32*, L24307, doi:10.1029/2005GL024188.

Dewey, J. W., G. Choy, B. Presgrave, S. Sipkin, A. C. Tarr, H. Benz, P. Earle, and D. Wald (2007), Seismicity associated with the Sumatra-Andaman Islands earthquake of 26 December 2004, *Bull. Seismol. Soc. Am.*, *97*, S25–S42, doi:10.1785/0120050626.

Diament, M., H. Harjono, K. Karta, C. Deplus, D. Dahrin, M. T. J. Zen, M. Gerard, O. Lassal, A. Martin, and J. Malod (1992), Mentawai fault zone off Sumatra: A new key to the geodynamics of western Indonesia, *Geology*, *20*(3), 259–262, doi:10.1130/0091-7613(1992)020<0259:MFZOSA>2.3.CO;2.

Dong, D., P. Fang, Y. Bock, M. K. Cheng, and S. Miyazaki (2002), Anatomy of apparent seasonal variations from GPS-derived site position time series, *J. Geophys. Res.*, *107*(B4), 2075, doi:10.1029/2001JB000573.

Duputel, Z., H. Kanamori, V. C. Tsai, L. Rivera, L. Meng, J.-P. Ampuero, and J. M. Stock (2012), The 2012 Sumatra great earthquake sequence, *Earth Planet. Sci. Lett.*, *351-352*, 247–257, doi:10.1016/j.epsl.2012.07.017.

Einarsson, I., A. Hoechner, R. Wang, and J. Kusche (2010), Gravity changes due to the Sumatra-Andaman and Nias earthquakes as detected by the GRACE satellites: A reexamination, *Geophys. J. Int.*, *183*(2), 733–747, doi:10.1111/j.1365-246X.2010.04756.x.

Ekström, G., M. Nettles, and A. M. Dziewoński (2012), The global CMT project 2004–2010: Centroid-moment tensors for 13,017 earthquakes, *Phys. Earth Planet. Inter.*, *200*, 1–9, doi:10.1016/j.pepi.2012.04.002.

Fauzi, R. McCaffrey, D. Wark, Sunaryo, and P. Y. Prih Haryadi (1996), Lateral variation in slab orientation beneath Toba Caldera, northern Sumatra, *Geophys. Res. Lett.*, *23*(5), 443–446, doi:10.1029/96GL00381.

Feigl, K. L., and W. Thatcher (2006), Geodetic observations of post-seismic transients in the context of the earthquake deformation cycle, *C. R. Geosci.*, *338*(14-15), 1012–1028, doi:10.1016/j.crte.2006.06.006.

Fitch, T. J. (1972), Plate convergence, transcurrent faults, and internal deformation adjacent to Southeast Asia and the western Pacific, *J. Geophys. Res.*, *77*(23), 4432–4460, doi:10.1029/JB077i023p04432.

Franke, D., M. Schnabel, S. Ladage, D. R. Tappin, S. Neben, Y. S. Djajadihardja, C. Müller, H. Kopp, and C. Gaedicke (2008), The great Sumatra-Andaman earthquakes – Imaging the boundary between the ruptures of the great 2004 and 2005 earthquakes, *Earth Planet. Sci. Lett.*, *269*(1-2), 118–130, doi:10.1016/j.epsl.2008.01.047.

Freed, A. M. (2007), Afterslip (and only afterslip) following the 2004 Parkfield, California, earthquake, *Geophys. Res. Lett.*, *34*, L06312, doi:10.1029/2006GL029155.

Freed, A. M., and R. Bürgmann (2004), Evidence of power-law flow in the Mojave desert mantle, *Nature*, *430* (6999), 548–551, doi:10.1038/nature02784.

Freed, A. M., R. Bürgmann, E. Calais, J. Freymueller, and S. Hreinsdóttir (2006), Implications of deformation following the 2002 Denali, Alaska, earthquake for postseismic relaxation processes and lithospheric rheology, *J. Geophys. Res.*, *111*, B01401, doi:10.1029/2005JB003894.

Fujii, Y., and K. Satake (2007), Tsunami source of the 2004 Sumatra-Andaman earthquake inferred from tide gauge and satellite data, *Bull. Seismol. Soc. Am.*, *97*(1A), S192–S207, doi:10.1785/0120050613.

Gahalaut, V. K., et al. (2008), GPS measurements of postseismic deformation in the Andaman-Nicobar region following the giant 2004 Sumatra-Andaman earthquake, *J. Geophys. Res.*, *113*, B08401, doi:10.1029/2007JB005511.

Geersen, J., J. M. Bull, L. C. McNeill, T. J. Henstock, C. Gaedicke, N. Chamot-Rooke, and M. Delescluse (2015), Pervasive deformation of an oceanic plate and relationship to large > M_w 8 intraplate earthquakes: The northern Wharton Basin, Indian Ocean, *Geology*, *43*(4), 359–362, doi:10.1130/G36446.1.

Graindorge, D., et al. (2008), Impact of lower plate structure on upper plate deformation at the NW Sumatran convergent margin from seafloor morphology, *Earth Planet. Sci. Lett.*, *275*(3-4), 201–210, doi:10.1016/j.epsl.2008.04.053.

Gunawan, E., T. Sagiya, T. Ito, F. Kimata, T. Tabei, Y. Ohta, I. Meilano, H. Z. Abidin, I. N. Agustan, and D. Sugiyanto (2014), A comprehensive model of postseismic deformation of the 2004 Sumatra-Andaman earthquake deduced from GPS observations in northern Sumatra, *J. Asian Earth Sci.*, *88*, 218–229, doi:10.1016/j.jseaes.2014.03.016.

Han, S.-C., J. Sauber, S. B. Luthcke, C. Ji, and F. F. Pollitz (2008), Implications of postseismic gravity change following the great 2004 Sumatra-Andaman earthquake from the regional harmonic analysis of GRACE intersatellite tracking data, *J. Geophys. Res.*, *113*, B11413, doi:10.1029/2008JB005705.

Hashimoto, M., N. Choosakul, M. Hashizume, S. Takemoto, H. Takiguchi, Y. Fukuda, and K. Fujimori (2006), Crustal deformations associated with the great Sumatra-Andaman earthquake deduced from continuous GPS observation, *Earth Planets and Space*, *58*(2), 127–139.

Hayes, G. P., D. J. Wald, and R. L. Johnson (2012), Slab1.0: A three-dimensional model of global subduction zone geometries, *J. Geophys. Res.*, *117*, B01302, doi:10.1029/2011JB008524.

Hearn, E. H. (2003), What can GPS data tell us about the dynamics of post-seismic deformation?, *Geophys. J. Int.*, *155* (3), 753–777, doi:10.1111/j.1365-246X.2003.02030.x.

Hearn, E. H., R. Bürgmann, and R. E. Reilinger (2002), Dynamics of Izmit earthquake postseismic deformation and loading of the Duzce earthquake hypocenter, *Bull. Seismol. Soc. Am.*, *92*(1), 172–193, doi:10.1785/0120000832.

Hill, E. M., et al. (2012), The 2010 M_w 7.8 Mentawai earthquake: Very shallow source of a rare tsunami earthquake determined from tsunami field survey and near-field GPS data, *J. Geophys. Res.*, *117*, B06402, doi:10.1029/2012JB009159.

Hill, E. M., H. Yue, S. Barbot, T. Lay, P. Tapponnier, I. Hermawan, J. Hubbard, P. Banerjee, L. Feng, D. H. Natawidjaja, and K. Sieh (2015), The 2012 M_w 8.6 Wharton Basin sequence: A cascade of great earthquakes generated by near-orthogonal, young, oceanic mantle faults, *J. Geophys. Res.*, doi:10.1029/2014JB011703.

Hoechner, A., A. Y. Babeyko, and S. V. Sobolev (2008), Enhanced GPS inversion technique applied to the 2004 Sumatra earthquake and tsunami, *Geophys. Res. Lett.*, *35*, L08310, doi:10.1029/2007GL033133.

Hoechner, A., S. V. Sobolev, I. Einarsson, and R. Wang (2011), Investigation on afterslip and steady state and transient rheology based on postseismic deformation and geoid change caused by the Sumatra 2004 earthquake, *Geochem. Geophys. Geosyst.*, *12*, Q07010, doi:10.1029/2010GC003450.

Hsu, Y.-J., M. Simons, J.-P. Avouac, J. Galetzka, K. Sieh, M. Chlieh, D. H. Natawidjaja, L. Prawirodirdjo, and Y. Bock (2006), Frictional afterslip following the 2005 Nias-Simeulue earthquake, Sumatra, *Science*, *312*(5782), 1921–1926, doi:10.1126/science.1126960.

Hu, Y., and K. Wang (2012), Spherical-Earth finite element model of short-term postseismic deformation following the 2004 Sumatra earthquake, *J. Geophys. Res.*, *117*, B05404, doi:10.1029/2012JB009153.

Hughes, K. L. H., T. Masterlark, and W. D. Mooney (2010), Poroelastic stress-triggering of the 2005 M8.7 Nias earthquake by the 2004 M9.2 Sumatra-Andaman earthquake, *Earth Planet. Sci. Lett.*, *293*(3-4), 289–299, doi:10.1016/j.epsl.2010.02.043.

Ishii, M., P. M. Shearer, H. Houston, and J. E. Vidale (2007), Teleseismic P wave imaging of the 26 December 2004 Sumatra-Andaman and 28 March 2005 Sumatra earthquake ruptures using the Hi-net array, *J. Geophys. Res.*, *112*, B11307, doi:10.1029/2006JB004700.

Jacob, J., J. Dyment, and V. Yatheesh (2014), Revisiting the structure, age, and evolution of the Wharton Basin to better understand subduction under Indonesia, *J. Geophys. Res. Solid Earth*, *119*(1), 169–190, doi:10.1002/2013JB010285.

Jónsson, S. (2008), Importance of post-seismic viscous relaxation in southern Iceland, *Nat. Geosci.*, *1*(2), 136–139, doi:10.1038/ngeo105.

Jónsson, S., P. Segall, R. Pedersen, and G. Björnsson (2003), Post-earthquake ground movements correlated to pore-pressure transients, *Science*, *424*(6945), 179–183, doi:10.1038/nature01776.

Konca, A. O., V. Hjorleifsdottir, T.-R. A. Song, J.-P. Avouac, D. V. Helmberger, C. Ji, K. Sieh, R. Briggs, and A. Meltzner (2007), Rupture kinematics of the 2005 M_w 8.6 Nias-Simeulue earthquake from the joint inversion of seismic and geodetic data, *Bull. Seismol. Soc. Am.*, *97*(1A), S307–S322, doi:10.1785/0120050632.

Konca, A. O., et al. (2008), Partial rupture of a locked patch of the Sumatra megathrust during the 2007 earthquake sequence, *Nature*, *456* (7222), 631–635, doi:10.1038/nature07572.

Kreemer, C., G. Blewitt, and F. Maerten (2006a), Co- and postseismic deformation of the 28 March 2005 Nias M_w 8.7 earthquake from continuous GPS data, *Geophys. Res. Lett.*, *33*, L07307, doi:10.1029/2005GL025566.

Kreemer, C., G. Blewitt, W. C. Hammond, and H.-P. Plag (2006b), Global deformation from the great 2004 Sumatra-Andaman Earthquake observed by GPS: Implications for rupture process and global reference frame, *Earth Planets Space*, *58*(2), 141–148.

Lange, D., F. Tilmann, A. Rietbrock, R. Collings, D. H. Natawidjaja, B. W. Suwargadi, P. Barton, T. Henstock, and T. Ryberg (2010), The fine structure of the subducted Investigator Fracture Zone in western Sumatra as seen by local seismicity, *Earth Planet. Sci. Lett.*, *298*(1-2), 47–56, doi:10.1016/j.epsl.2010.07.020.

Lay, T., et al. (2005), The great Sumatra-Andaman earthquake of 26 December 2004, *Science*, *308* (5725), 1127–1133, doi:10.1126/science.1112250.

Lay, T., C. J. Ammon, H. Kanamori, Y. Yamazaki, K. F. Cheung, and A. R. Hutko (2011), The 25 October 2010 Mentawai tsunami earthquake (M_w 7.8) and the tsunami hazard presented by shallow megathrust ruptures, *Geophys. Res. Lett.*, *38*, L06302, doi:10.1029/2010GL046552.

Lorito, S., A. Piatanesi, V. Cannelli, F. Romano, and D. Melini (2010), Kinematics and source zone properties of the 2004 Sumatra-Andaman earthquake and tsunami: Nonlinear joint inversion of tide gauge, satellite altimetry, and GPS data, *J. Geophys. Res.*, *115*, B02304, doi:10.1029/2008JB005974.

Lubis, A. M., A. Hashima, and T. Sato (2013), Analysis of afterslip distribution following the 2007 September 12 southern Sumatra earthquake using poroelastic and viscoelastic media, *Geophys. J. Int.*, *192*(1), 18–37, doi:10.1093/gji/ggs020.

Lyard, F., F. Lefevre, T. Letellier, and O. Francis (2006), Modelling the global ocean tides: Modern insights from FES2004, *Ocean Dyn.*, *56*(5-6), 394–415, doi:10.1007/s10236-006-0086-x.

Malod, J. A., and B. M. Kemal (1996), The Sumatra margin: Oblique subduction and lateral displacement of the accretionary prism, *Geol. Soc. London, Spec. Publ.*, *106*(1), 19–28, doi:10.1144/GSL.SP.1996.106.01.03.

Marone, C. J., C. H. Scholz, and R. Bilham (1991), On the mechanics of earthquake afterslip, *J. Geophys. Res.*, *96* (B5), 8441–8452, doi:10.1029/91JB00275.

McCaffrey, R. (1991), Slip vectors and stretching of the Sumatran fore arc, *Geology*, *19* (9), 881–884, doi:10.1130/0091-7613(1991)019<0881:SVASOT>2.3.CO;2.

McCaffrey, R. (1992), Oblique plate convergence, slip vectors, and forearc deformation, *J. Geophys. Res.*, *97*(B6), 8905–8915, doi:10.1029/92JB00483.

McCloskey, J., D. Lange, F. Tilmann, S. S. Nalbant, A. F. Bell, D. H. Natawidjaja, and A. Rietbrock (2010), The September 2009 Padang earthquake, *Nat. Geosci.*, *3*(2), 70–71, doi:10.1038/ngeo753.

Meltzner, A. J., K. Sieh, M. Abrams, D. C. Agnew, K. W. Hudnut, J.-P. Avouac, and D. H. Natawidjaja (2006), Uplift and subsidence associated with the great Aceh-Andaman earthquake of 2004, *J. Geophys. Res.*, *111*, B02407, doi:10.1029/2005JB003891.

Meltzner, A. J., K. Sieh, H.-W. Chiang, C.-C. Shen, B. W. Suwargadi, D. H. Natawidjaja, B. E. Philibosian, R. W. Briggs, and J. Galetzka (2010), Coral evidence for earthquake recurrence and an A.D. 1390–1455 cluster at the south end of the 2004 Aceh-Andaman rupture, *J. Geophys. Res.*, *115*, B10402, doi:10.1029/2010JB007499.

Meltzner, A. J., K. Sieh, H.-W. Chiang, C.-C. Shen, B. W. Suwargadi, D. H. Natawidjaja, B. Philibosian, and R. W. Briggs (2012), Persistent termini of 2004- and 2005-like ruptures of the Sunda megathrust, *J. Geophys. Res.*, *117*, B04405, doi:10.1029/2011JB008888.

Meng, L., J.-P. Ampuero, J. Stock, Z. Duputel, Y. Luo, and V. C. Tsai (2012), Earthquake in a maze: Compressional rupture branching during the 2012 M_w 8.6 Sumatra earthquake, *Science*, *337*(6095), 724–726, doi:10.1126/science.1224030.

Nakano, M., H. Kumagai, S. Toda, R. Ando, T. Yamashina, H. Inoue, and Sunarjo (2010), Source model of an earthquake doublet that occurred in a pull-apart basin along the Sumatran fault, Indonesia, *Geophys. J. Int.*, *181*(1), 141–153, doi:10.1111/j.1365-246X.2010.04511.x.

Newman, A. V., G. Hayes, Y. Wei, and J. Convers (2011), The 25 October 2010 Mentawai tsunami earthquake, from real-time discriminants, finite-fault rupture, and tsunami excitation, *Geophys. Res. Lett.*, *38*, L05302, doi:10.1029/2010GL046498.

Nishimura, T., T. Hirasawa, S. Miyazaki, T. Sagiya, T. Tada, S. Miura, and K. Tanaka (2004), Temporal change of interplate coupling in northeastern Japan during 1995–2002 estimated from continuous GPS observations, *Geophys. J. Int.*, *157* (2), 901–916, doi:10.1111/j.1365-246X.2004.02159.x.

Nur, A., and G. Mavko (1974), Postseismic viscoelastic rebound, *Science*, *183*(4121), 204–206, doi:10.1126/science.183.4121.204.

Ogawa, R., and K. Heki (2007), Slow postseismic recovery of geoid depression formed by the 2004 Sumatra-Andaman Earthquake by mantle water diffusion, *Geophys. Res. Lett.*, *34*, L06313, doi:10.1029/2007GL029340.

Panet, I., F. Pollitz, V. Mikhailov, M. Diament, P. Banerjee, and K. Grijalva (2010), Upper mantle rheology from GRACE and GPS postseismic deformation after the 2004 Sumatra-Andaman earthquake, *Geochem. Geophys. Geosyst.*, *11*(6), 1–20, doi:10.1029/2009GC002905.

Panumastrakul, E., W. J. F. Simons, and C. Satirapod (2012), Modelling post-seismic displacements in Thai geodetic network due to the Sumatra-Andaman and Nias earthquakes using GPS observations, *Surv. Rev.*, *44*(324), 72–77, doi:10.1179/1752270611Y.0000000017.

Paul, J., A. R. Lowry, R. Bilham, S. Sen, and R. Smalley (2007), Postseismic deformation of the Andaman Islands following the 26 December, 2004 Great Sumatra-Andaman earthquake, *Geophys. Res. Lett.*, *34*, L19309, doi:10.1029/2007GL031024.

Paul, J., C. P. Rajendran, A. R. Lowry, V. Andrade, and K. Rajendran (2012), Andaman postseismic deformation observations: Still slipping after all these years?, *Bull. Seismol. Soc. Am.*, *102*(1), 343–351, doi:10.1785/0120110074.

Peltzer, G., P. Rosen, F. Rogez, and K. Hudnut (1996), Postseismic rebound in fault step-overs caused by pore fluid flow, *Science*, *273*(5279), 1202–1204, doi:10.1126/science.273.5279.1202.

Peltzer, G., P. Rosen, F. Rogez, and K. Hudnut (1998), Poroelastic rebound along the Landers 1992 earthquake surface rupture, *J. Geophys. Res.*, *103*(B12), 30,131–30,145, doi:10.1029/98JB02302.

Perfettini, H., and J.-P. Avouac (2004), Postseismic relaxation driven by brittle creep: A possible mechanism to reconcile geodetic measurements and the decay rate of aftershocks, application to the Chi-Chi earthquake, Taiwan, *J. Geophys. Res.*, *109*, B02304, doi:10.1029/2003JB002488.

Perfettini, H., J.-P. Avouac, and J.-C. Ruegg (2005), Geodetic displacements and aftershocks following the 2001 $M_w = 8.4$ Peru earthquake: Implications for the mechanics of the earthquake cycle along subduction zones, *J. Geophys. Res.*, *110*, B09404, doi:10.1029/2004JB003522.

Pesicek, J. D., C. H. Thurber, H. Zhang, H. R. DeShon, E. R. Engdahl, and S. Widiyantoro (2010), Teleseismic double-difference relocation of earthquakes along the Sumatra-Andaman subduction zone using a 3-D model, *J. Geophys. Res.*, *115*, B10303, doi:10.1029/2010JB007443.

Pollitz, F., P. Banerjee, K. Grijalva, B. Nagarajan, and R. Bürgmann (2008), Effect of 3-D viscoelastic structure on post-seismic relaxation from the 2004 M = 9.2 Sumatra earthquake, *Geophys. J. Int.*, *173*(1), 189–204, doi:10.1111/j.1365-246X.2007.03666.x.

Pollitz, F. F., G. Peltzer, and R. Bürgmann (2000), Mobility of continental mantle: Evidence from postseismic geodetic observations following the 1992 Landers earthquake, *J. Geophys. Res.*, *105*(B4), 8035–8054, doi:10.1029/1999JB900380.

Pollitz, F. F., C. Wicks, and W. Thatcher (2001), Mantle flow beneath a continental strike-slip fault: Postseismic deformation after the 1999 Hector Mine earthquake, *Science*, *293*(5536), 1814–1818, doi:10.1126/science.1061361.

Pollitz, F. F., R. Bürgmann, and P. Banerjee (2006), Post-seismic relaxation following the great 2004 Sumatra-Andaman earthquake on a compressible self-gravitating Earth, *Geophys. J. Int.*, *167*(1), 397–420, doi:10.1111/j.1365-246X.2006.03018.x.

Prawirodirdjo, L., Y. Bock, J. F. Genrich, S. S. O. Puntodewo, J. Rais, C. Subarya, and S. Sutisna (2000), One century of tectonic deformation along the Sumatran fault from triangulation and Global Positioning System surveys, *J. Geophys. Res.*, *105* (B12), 28,343–28,361, doi:10.1029/2000JB900150.

Prawirodirdjo, L., R. McCaffrey, C. D. Chadwell, Y. Bock, and C. Subarya (2010), Geodetic observations of an earthquake cycle at the Sumatra subduction zone: Role of interseismic strain segmentation, *J. Geophys. Res.*, *115*, B03414, doi:10.1029/2008JB006139.

Rhie, J., D. Dreger, R. Bürgmann, and B. Romanowicz (2007), Slip of the 2004 Sumatra-Andaman earthquake from joint inversion of long-period global seismic waveforms and GPS static offsets, *Bull. Seismol. Soc. Am.*, *97*, S115–S127, doi:10.1785/0120050620.

Rivera, L., K. Sieh, D. Helmberger, and D. Natawidjaja (2002), A comparative study of the Sumatran Subduction-Zone earthquakes of 1935 and 1984, *Bull. Seismol. Soc. Am.*, *92*(5), 1721–1736.

Robinson, D. P., C. Henry, S. Das, and J. H. Woodhouse (2001), Simultaneous rupture along two conjugate planes of the Wharton Basin earthquake, *Science*, *292*(5519), 1145–1148, doi:10.1126/science.1059395.

Rousset, B., S. Barbot, J.-P. Avouac, and Y.-J. Hsu (2012), Postseismic deformation following the 1999 Chi-Chi earthquake, Taiwan: Implication for lower-crust rheology, *J. Geophys. Res.*, *117*, B12405, doi:10.1029/2012JB009571.

Samuel, M. A., and N. A. Harbury (1996), The Mentawai fault zone and deformation of the Sumatran Forearc in the Nias area, *Geol. Soc. London Spec. Publ.*, *106*(1), 337–351, doi:10.1144/GSL.SP.1996.106.01.22.

Satake, K., Y. Nishimura, P. S. Putra, A. R. Gusman, H. Sunendar, Y. Fujii, Y. Tanioka, H. Latief, and E. Yulianto (2012), Tsunami source of the 2010 Mentawai, Indonesia earthquake inferred from tsunami field survey and waveform modeling, *Pure Appl. Geophys.*, *170*(9-10), 1567–1582, doi:10.1007/s00024-012-0536-y.

Satirapod, C., I. Trisirisatayawong, L. Fleitout, J. D. Garaud, and W. J. F. Simons (2013), Vertical motions in Thailand after the 2004 Sumatra-Andaman earthquake from GPS observations and its geophysical modelling, *Adv. Space Res.*, *51*(8), 1565–1571, doi:10.1016/j.asr.2012.04.030.

Satriano, C., E. Kiraly, P. Bernard, and J.-P. Vilotte (2012), The 2012 M_w 8.6 Sumatra earthquake: Evidence of westward sequential seismic ruptures associated to the reactivation of a N-S ocean fabric, *Geophys. Res. Lett.*, *39*, L15302, doi:10.1029/2012GL052387.

Savage, J. C. (1990), Equivalent strike-slip earthquake cycles in half-space and lithosphere-asthenosphere earth models, *J. Geophys. Res.*, *95*(B4), 4873–4879, doi:10.1029/JB095iB04p04873.

Savage, J. C., and J. Langbein (2008), Postearthquake relaxation after the 2004 M6 Parkfield, California, earthquake and rate-and-state friction, *J. Geophys. Res.*, *113*, B10407, doi:10.1029/2008JB005723.

Savage, J. C., and J. L. Svarc (2009), Postseismic relaxation following the 1992 M7.3 Landers and 1999 M7.1 Hector Mine earthquakes, southern California, *J. Geophys. Res.*, *114*, B01401, doi:10.1029/2008JB005938.

Savage, J. C., J. L. Svarc, and S.-B. Yu (2005), Postseismic relaxation and transient creep, *J. Geophys. Res.*, *110*, B11402, doi:10.1029/2005JB003687.

Savage, J. C., J. L. Svarc, and S.-B. Yu (2007), Postseismic relaxation and aftershocks, *J. Geophys. Res.*, *112*, B06406, doi:10.1029/2006JB004584.

Schmid, R., P. Steigenberger, G. Gendt, M. Ge, and M. Rothacher (2007), Generation of a consistent absolute phase-center correction model for GPS receiver and satellite antennas, *J. Geod.*, *81*(12), 781–798, doi:10.1007/s00190-007-0148-y.

Sieh, K., and D. H. Natawidjaja (2000), Neotectonics of the Sumatran fault, Indonesia, *J. Geophys. Res.*, *105*(B12), 28,295–28,326, doi:10.1029/2000JB900120.

Sladen, A., and H. Hébert (2008), On the use of satellite altimetry to infer the earthquake rupture characteristics: Application to the 2004 Sumatra event, *Geophys. J. Int.*, *172*(2), 707–714, doi:10.1111/j.1365-246X.2007.03669.x.

Subarya, C., M. Chlieh, L. Prawirodirdjo, J.-P. Avouac, Y. Bock, K. Sieh, A. J. Meltzner, D. H. Natawidjaja, and R. McCaffrey (2006), Plate-boundary deformation associated with the great Sumatra-Andaman earthquake, *Nature*, *440*(7080), 46–51, doi:10.1038/nature04522.

Taylor, J. R. (1997), *An Introduction to Error Analysis: The Study of Uncertainties in Physical Measurements*, 2nd ed., 327 pp., Univ. Science Books, Sausalito, Calif.

Thatcher, W. (1983), Nonlinear strain buildup and the earthquake cycle on the San Andreas Fault, *J. Geophys. Res.*, *88*(B7), 5893–5902, doi:10.1029/JB088iB07p05893.

Tilmann, F. J., T. J. Craig, I. Grevemeyer, B. Suwargadi, H. Kopp, and E. Flueh (2010), The updip seismic/aseismic transition of the Sumatra megathrust illuminated by aftershocks of the 2004 Aceh-Andaman and 2005 Nias events, *Geophys. J. Int.*, *181*(3), 1261–1274, doi:10.1111/j.1365-246X.2010.04597.x.

Tobita, M., H. Suito, T. Imakiire, M. Kato, S. Fujiwara, and M. Murakami (2006), Outline of vertical displacement of the 2004 and 2005 Sumatra earthquakes revealed by satellite radar imagery, *Earth Planets Space*, *58*(12), e1–e4.

Untung, M., N. Buyung, E. Kertapati, Undang, and C. R. Allen (1985), Rupture along the Great Sumatran fault, Indonesia, during the earthquakes of 1926 and 1943, *Bull. Seismol. Soc. Am.*, *75*(1), 313–317.

Vigny, C., et al. (2005), Insight into the 2004 Sumatra-Andaman earthquake from GPS measurements in southeast Asia, *Nature*, *436*(7048), 201–206, doi:10.1038/nature03937.

Walker, K. T., M. Ishii, and P. M. Shearer (2005), Rupture details of the 28 March 2005 Sumatra M_w 8.6 earthquake imaged with teleseismic P waves, *Geophys. Res. Lett.*, *32*, L24303, doi:10.1029/2005GL024395.

Wei, S., D. Helmberger, and J.-P. Avouac (2013), Modeling the 2012 Wharton basin earthquakes off-Sumatra: Complete lithospheric failure, *J. Geophys. Res. Solid Earth*, *118*(7), 3592–3609, doi:10.1002/jgrb.50267.

Wessel, P., W. H. F. Smith, R. Scharroo, J. Luis, and F. Wobbe (2013), Generic mapping tools: Improved version released, *Eos Trans. AGU*, *94*(45), 409–410, doi:10.1002/2013EO450001.

Wiseman, K., P. Banerjee, K. Sieh, R. Bürgmann, and D. H. Natawidjaja (2011), Another potential source of destructive earthquakes and tsunami offshore of Sumatra, *Geophys. Res. Lett.*, *38*, L10311, doi:10.1029/2011GL047226.

Wiseman, K., P. Banerjee, R. Bürgmann, K. Sieh, D. S. Dreger, and I. Hermawan (2012), Source model of the 2009 M_w 7.6 Padang intraslab earthquake and its effect on the Sunda megathrust, *Geophys. J. Int.*, *190*(3), 1710–1722, doi:10.1111/j.1365-246X.2012.05600.x.

Yue, H., T. Lay, and K. D. Koper (2012), En échelon and orthogonal fault ruptures of the 11 April 2012 great intraplate earthquakes, *Nature*, *490*(7419), 245–249, doi:10.1038/nature11492.

Yue, H., T. Lay, L. Rivera, Y. Bai, Y. Yamazaki, K. F. Cheung, E. M. Hill, K. Sieh, W. Kongko, and A. Muhari (2014), Rupture process of the 2010 M_w 7.8 Mentawai tsunami earthquake from joint inversion of near-field hr-GPS and teleseismic body wave recordings constrained by tsunami observations, *J. Geophys. Res. Solid Earth*, *119*(7), 5574–5593, doi:10.1002/2014JB011082.

Zumberge, J. F., M. B. Heflin, D. C. Jefferson, M. M. Watkins, and F. H. Webb (1997), Precise point positioning for the efficient and robust analysis of GPS data from large networks, *J. Geophys. Res.*, *102*(B3), 5005–5017, doi:10.1029/96JB03860.